This is a repository copy of *Acoustic waves in a halfspace material filled with random particulate*.

White Rose Research Online URL for this paper:
https://eprints.whiterose.ac.uk/221349/

Version: Published Version

PAPER • OPEN ACCESS

Acoustic waves in a halfspace material filled with random particulate

View the article online for updates and enhancements.

PAPER

CrossMark

Acoustic waves in a halfspace material filled with random particulate

Paulo S Piva[*] , Kevish K Napal and Art L Gower

Department of Mechanical Engineering, The University of Sheffield, Sheffield, United Kingdom
[*] Author to whom any correspondence should be addressed.

E-mail: pspiva1@sheffield.ac.uk

Abstract

Particulate materials include powders, emulsions, composites, and many others. This is why measuring these has become important for both industry and scientific applications. For industrial applications, the greatest need is to measure dense particulates, *in-situ*, and non-destructively. In theory, this could be achieved with acoustics: the standard method is to send an acoustic wave through the particulate and then attempt to measure the effective wave speed and attenuation. A major obstacle here is that it is not clear how to relate the effective wave speed and attenuation to the reflection and transmission coefficients, which are far easier to measure. This is because it has been very difficult to mathematically account for different background mediums. In this paper, we resolve this obstacle. To help comprehension, we present how to account for different background mediums for a simple case: a halfspace filled with a random particulate, where the background of the halfspace is different from the exterior medium. The key to solving this problem was to derive a systematic extension of a widely used closure approximation: the quasi-crystalline approximation. We present some numerical results to demonstrate that the reflection coefficient can be easily calculated for a broad range of frequencies and particle properties.

1. Introduction

Particulate materials are composed of small particles embedded in a continuous medium, like a powder in air, emulsions such as oil droplets in water, or air bubbles appearing in boiling water. Many applications, for example sensing, require a descriptive model of particulate materials. The positions of the particles are disordered and are either not known or cannot be completely controlled. Therefore, the most important features of particulate materials are statistical, such as the average particle size or inter-particle distance.

Sensing. Non-destructive measurements of particle size and properties can be achieved using wave scattering (acoustic, electromagnetic or elastic) [Cha+05, AC15, FHP16, 20917]. Characterising, or monitoring, the particles is needed to ensure quality, or can be used in feedback loops during production or manufacturing. As the particles can change position (or even properties) in time, to obtain a reliable measurement, experiments need to be repeated many times to then compute the average wave response. This average response depends only on the statistical properties, such as average concentration and particle size, which are usually the most important features for industrial applications. Mathematically, the result of averaging over measurements in time (or space) can be equivalent to a procedure called ensemble averaging, which we use in this work, see [Fol45, Mis+16, Hua63] for details.

Broad frequency range. To sense the size of particles, we need to consider a broad range of frequencies, so that the wavelengths are comparable to the particle size. It is not enough to develop a theory for only the low frequency limit, as in this limit it is not possible to sense particle size distribution. For example, in the long wavelength limit (low frequency) for acoustics [CDW12], the material is completely described by two

Figure 1. Shows the cross-section of a pipe, with a fluid flowing in the direction of the black arrow. Particles are suspended in the fluid, represented by black circles. A pair of transducers (acoustic sensors) are attached to the pipe walls. One transducer emits waves and measures their reflection, while the other measures the transmitted wave. This illustration is just a pictorial representation. For any real applications, particles would be much smaller and more numerous. The figure was generated in Julia with the MultipleScattering.jl library [GD24, Pau24].

numbers: the effective density and effective bulk modulus [Gow+18]. So, in terms of sensing, to learn more than just two numbers from a wave experiment we need to consider shorter wavelengths.

Effective Waves Method. As we need a broad range of frequencies, we make use of a method called the *Effective Waves Method* [GK21, GHK23, NPG24], which can account for wave scattering in dense or sparse particulate materials for a broad range of frequencies (see [KPG24] for phase diagrams). This method accounts for multiple scattering between all particles, and provides a way to perform sensitivity studies on a wide range of parameters such as particle size distribution and volume fraction.

Different background mediums. When using the Effective Waves Method to design ways to sense particles we came across a significant barrier: it is not clear how to calculate the average scattering when the source comes from a medium which is different from the background medium of the particles. An example is shown in figure 1, which depicts an emulsion (particles in a fluid) travelling along a metal pipe. The pipe material is different from the background fluid. There have been work, and experiments, in the literature that considers the case of different background mediums [Faw21, Gar+05, Sim+24], but the expressions used do not come from first principles calculations. We discuss this further in the literature review below. To design robust sensing methods, we need to account for these different mediums, which is the main goal of this paper. After significant calculations from first principles, we arrive at a simple strategy which will lead to more robust sensing methods.

Quasi-crystalline approximation. To solve for all orders of multiple scattering between particles, on average, one needs to use a closure approximation [Ado71, Kue16]. The most standard closure assumption to account for scattering between particles is called the Quasi-Crystalline Approximation (QCA) [Lax52, MVV84, GPA19]. We derive a consistent extension to QCA (named X-QCA) to also account for scattering between particles and interfaces. To summarise, eXtended Quasi-Crystalline Approximation (X-QCA) accounts for the same scattering orders as QCA and leads to simpler calculations. For clarity, we consider only a simple case: plane wave incidence on a halfspace filled with random particles (see figure 4), and only for acoustic wave scattering.

Further applications. Other than sensing, accounting for scattering between layers and particles can lead to improved design of: graded particulate materials [Miy+99] and disordered metamaterials with tailored frequency response. Disordered particulate materials can be far simpler to manufacture on a large scale,

because the exact positioning of the particles does not need to be carefully controlled, as it does in most periodic metamaterials.

A brief literature review. Most of the work done in particulates and composites is focused on the low frequency limit, for example [PA10], or for broader frequencies but with only one background medium [CDW12, CD15, LM05, LM06].

Recent work on acoustic scattering by random composite media has been carried out by John R. Willis [Wil19, Wil20, Wil23], in which a broad frequency response is considered. According to [Wil19], the model framework is based on elasticity [Wil81], and it describes wave scattering (acoustic or elastic) from a halfspace formed by three distinct phases. Compared to figure 3 later in the text, one phase would be represented by the exterior medium (blue), the second could be thought of as the matrix (yellow), and the last as the particles (black circles). However, the distribution of each phase in the halfspace is given in terms of a two-point correlation function, and not by placing particles as shown in figures 1 and 3. To solve the resulting equations, Willis assumed two of the phases have the same bulk modulus in [Wil23]. In this paper, we do not impose any restrictions on the acoustic properties of the three phases.

In this work we follow a first principles approach similar to [KW20], which accounts for all orders of multiple scattering. To solve for the average reflected and transmitted waves, Kristensson and Wellander [KW20] used the standard QCA (for scattering between particles) and specialised to either a low particle volume fraction or low frequency. In contrast, in this paper, we do not need to specialise to a low particle volume fraction or low frequency and reach solutions which are easier to compute and are, in principle, as accurate. To achieve this we deduce an extension of the quasi-crystalline approximation (X-QCA), which simplifies the scattering between particles and walls.

Summary of the paper. In section 1.1 we introduce an overview of how to account for multiple scattering between particles and interfaces for the average wave in materials with random microstructure. In section 2 we define the setup of a plane wave incident on a halfspace filled with particles. In section 3 we explicitly write the system of equations of the problem for acoustic scattering of waves for one configuration of particles. In section 4 we define the probability density of each realisation, and all the statistical assumptions used throughout the paper. In section 5 we compute the average of the total pressure field and apply boundary conditions on the interface between the different mediums in the halfspace. In section 6 we use X-QCA to determine the average of the backscattering operator to make a clear connection with the strategy introduced in section 1.1. In section 7 we derive X-QCA, which can be used in the presence of different background mediums. In section 8 we apply the Effective Waves Method and present the numerical results achieved.

1.1. Overview of the strategy

In this section, we show how to intuitively deduce wave scattering from a random particulate in the presence of different background mediums. We do this for the simplest scenario: plane wave scattering. After this section, we deduce rigorously the results presented here.

Let $\boldsymbol{r} = (x, y, z)$ be a position in $\mathbb{R}^3$. Consider a homogeneous acoustic halfspace, which we call the background matrix, occupying the region $z > 0$, in $\mathbb{R}^3$, which is filled with a random complex material.

Consider another homogeneous acoustic halfspace $z < 0$ which has different properties to the background matrix in $z > 0$. From the region $z < 0$, an incident plane wave propagates in the positive z direction given by

$$u_{\text{in}}(\boldsymbol{r}) = G e^{ikz}$$

with $k > 0$ being the wavenumber of the $z < 0$ region.

Surprisingly, to describe the average transmitted and reflected waves due to the incident plane wave is not straightforward, and arguably unsolved when considering all the multiple scattering between the interface and embedded random medium. During our work, we realised a simple intuitive trick to arrive at the same results achieved by the first principles calculations. The idea is to use what is already known: the solution of an average reflected plane wave from a complex material that is embedded in just one homogeneous medium. To use this solution, we consider an artificial region $0 < z < \delta$ which is homogeneous and has the same properties as the background matrix. See figure 2(a) for an illustration.

For just one realisation of the complex material, i.e. the deterministic case, the total acoustic field is given by

$$u_{\text{tot}}(\boldsymbol{r}) = \begin{cases} G e^{ikz} + R e^{-ikz} + \varepsilon_-(\boldsymbol{r}), & z < 0 \\ A e^{ik_0 z} + B e^{-ik_0 z} + \varepsilon_+(\boldsymbol{r}), & 0 < z < \delta \end{cases} \tag{1}$$
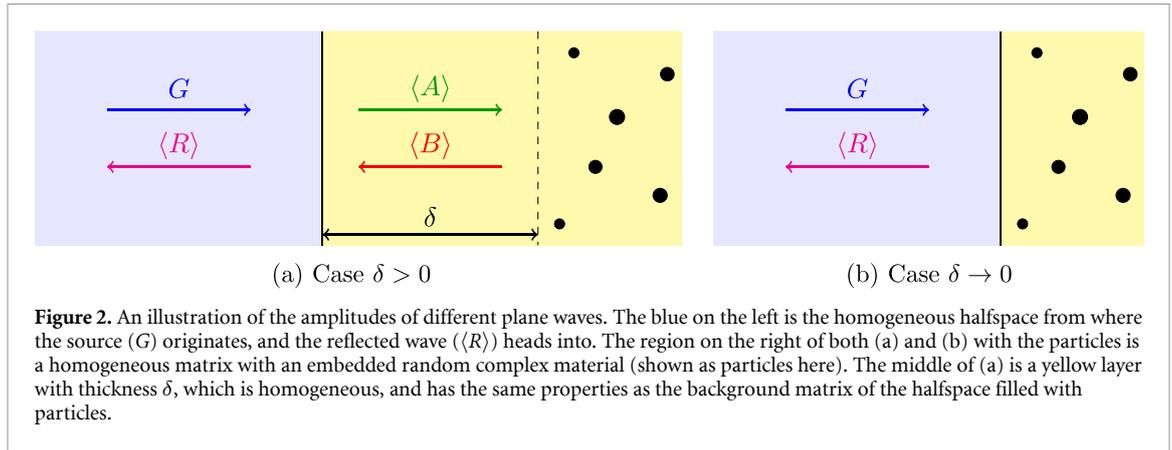
Figure 2. An illustration of the amplitudes of different plane waves. The blue on the left is the homogeneous halfspace from where the source (G) originates, and the reflected wave ($\langle R \rangle$) heads into. The region on the right of both (a) and (b) with the particles is a homogeneous matrix with an embedded random complex material (shown as particles here). The middle of (a) is a yellow layer with thickness δ, which is homogeneous, and has the same properties as the background matrix of the halfspace filled with particles.

where k_0 is the wavenumber of the region $0 < z < \delta$, and $G, R, A, B \in \mathbb{C}$ are the amplitudes of the: incident plane wave, reflected plane wave, and two transmitted plane waves, respectively. The terms $\varepsilon_\pm(\boldsymbol{r})$ represent the non-planar contribution from the random material. This non-planar contribution will be zero later when taking an ensemble average over the random variables.

We can calculate the unknown amplitudes by applying standard transmission boundary conditions across $z = 0$ given by

$$\begin{cases} u_{\text{tot}}(\boldsymbol{r}) \text{ is continuous at } z = 0, \\ \dfrac{1}{\rho(\boldsymbol{r})} \dfrac{\partial}{\partial z} u_{\text{tot}}(\boldsymbol{r}) \text{ is continuous at } z = 0, \end{cases} \tag{2}$$

where $\rho(\boldsymbol{r})$ is the density of the medium.

Let us attempt to use (2) to deduce the average reflection. To describe averages, we introduce the random variable σ to denote one realisation (or configuration) of this random material. For example, in a material composed of small particles σ represents one possible configuration of the particles and their acoustic properties, see figure 2(b). In this sense, the ensemble average $\langle \circ \rangle$ gives the average of $\circ$ over all possible realisations σ. Later we define this in detail.

Returning to (1), we know that on average $\langle \varepsilon_\pm(\boldsymbol{r}) \rangle = 0$ due to planar symmetry. Performing the ensemble average of both sides of (1) then leads to

$$\langle u_{\text{tot}}(\boldsymbol{r}) \rangle = \begin{cases} G e^{ikz} + \langle R \rangle e^{-ikz}, & z < 0, \\ \langle A \rangle e^{ik_0 z} + \langle B \rangle e^{-ik_0 z}, & 0 < z < \delta, \end{cases}$$

where $\langle G \rangle = G$ because the incident wave is the same for each realisation σ. Figure 2(a) shows how each plane wave contributes to the average field. The goal is to first solve the case shown in figure 2(a) and then take the limit $\delta \to 0$ to reach the solution of the case shown in figure 2(b).

Taking an ensemble average on both side of the boundary conditions (2), after some algebra, results in

$$\begin{cases} \langle R \rangle = \zeta_R G + \zeta_T \langle B \rangle, \\ \langle A \rangle = \gamma_0 \zeta_T G - \zeta_R \langle B \rangle, \end{cases} \tag{3}$$

with ζ_R, ζ_T and γ_0 being constants that depend on the material properties of the background mediums and are provided in section 5.2.

With the system (3), we have 3 unknowns: $\langle R \rangle$, $\langle B \rangle$, $\langle A \rangle$, but only 2 equations. We need another equation. We can obtain another equation by knowing how the particles themselves reflect a plane wave. The transmitted wave with amplitude A is reflected, in some sense, by the particulate material in the region $z > \delta$, and creates the reflected wave with amplitude B. This reflection is linear and can be represented by some scalar $\mathbb{T}_\sigma$ such that

$$\mathbb{T}_\sigma A := B. \tag{4}$$

We call $\mathbb{T}_\sigma$ the backscattering operator, and it depends on each realisation σ. See [GPA19, GK21] for examples of the average of this operator.

The main issue now is that taking an ensemble average on both sides of (4) results in

$$\langle B \rangle = \langle \mathbb{T}_\sigma A \rangle, \tag{5}$$
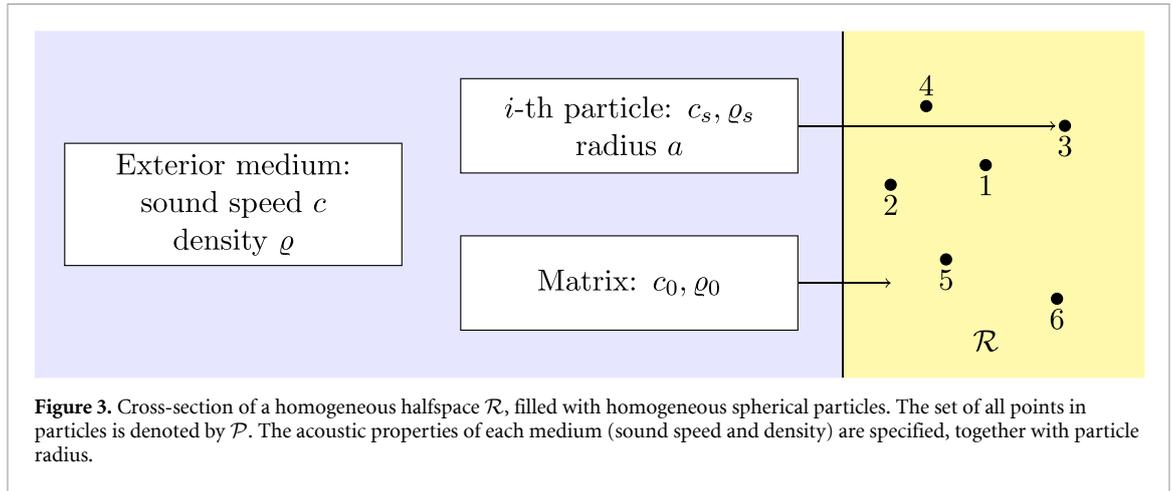
Figure 3. Cross-section of a homogeneous halfspace $\mathcal{R}$, filled with homogeneous spherical particles. The set of all points in particles is denoted by $\mathcal{P}$. The acoustic properties of each medium (sound speed and density) are specified, together with particle radius.

which does provide another equation, but also delivers another unknown $\langle \mathbb{T}_\sigma A \rangle$, which can not be written directly in terms of $\langle A \rangle$. This is because the waves A and B have been reflected between the complex random material and the interface at $z = 0$, so both of these waves do depend on the realisation σ. If the background matrix medium (yellow) was the same as the exterior (blue) medium, both shown in figure 2, then A would be the incident wave ($A = G$) and we would have $\langle \mathbb{T}_\sigma A \rangle = \langle \mathbb{T}_\sigma \rangle A$, as the incident wave does not depend on the realisation σ.

To resolve this, it is normal to assume a closure relation [Ado71, Kue16]. The simplest and most commonly used is a naive mean field approximation [KS20], given by

$$\langle B \rangle = \langle \mathbb{T}_\sigma A \rangle \approx \langle \mathbb{T}_\sigma \rangle \langle A \rangle. \tag{6}$$

At first, this approximation may appear crude. However, we will show in this paper that (6) is equivalent to the QCA. Therefore, when QCA is assumed, it would not be useful (or consistent) to use a more accurate approximation than (6).

The main goal of this work is to show that closure approximations of the form (6) can be deduced from first principles when using the same assumptions as QCA. Beyond just scattering by a halfspace, our approach leads to a general strategy to calculate (on average) multiple scattering between random particles and different background mediums.

2. Setting of the problem

Our aim is to describe wave scattering from a halfspace,

$$\mathcal{R} := \left\{ \boldsymbol{r} = (x, y, z) \in \mathbb{R}^3 \,|\, z \geqslant 0 \right\},$$

filled with particles. The region that all particles occupy is denoted by $\mathcal{P} \subset \mathcal{R}$, which is the union of non-overlapping homogeneous spheres with radius $a > 0$, sound speed $c_s \in \mathbb{C}$ and density $\varrho_s \in \mathbb{R}$[1].

We call the region in between all the particles, $\mathcal{R} \setminus \mathcal{P}$, the matrix, and the region $z < 0$ the exterior medium, from where the incident wave originates. See figure 3 for an illustration. The exterior medium has a speed of sound $c \in \mathbb{R}$ and density $\varrho \in \mathbb{R}$, while the matrix has homogeneous acoustic properties, $c_0 \in \mathbb{R}$ and $\varrho_0 \in \mathbb{R}$.

The pressure field in the frequency domain is denoted by u_{tot} and it satisfies the following Helmholtz equations:

$$\nabla^2 u_{\text{tot}}(\boldsymbol{r}) + k^2 u_{\text{tot}}(\boldsymbol{r}) = 0, \quad \text{for} \quad \boldsymbol{r} \notin \mathcal{R},$$
$$\nabla^2 u_{\text{tot}}(\boldsymbol{r}) + k_0^2 u_{\text{tot}}(\boldsymbol{r}) = 0, \quad \text{for} \quad \boldsymbol{r} \in \mathcal{R} \setminus \mathcal{P},$$

where $\omega \in \mathbb{R}$ is the angular frequency, $k := \omega/c$ is the wavenumber for the exterior medium (blue region), $k_0 := \omega/c_0$ is the wavenumber for the matrix (yellow region).

---

[1] It is not difficult to generalize all results presented here for the multispecies case, where each particle can have a different radius, sound speed and density. The procedure would be the same as done in [GK21].

Figure 4. Shows the different waves that are scattered from, and arrive at, the particles and the boundary of $\mathcal{R}$. Each arrow identifies where the wave was generated and what it excites. The colour of each arrow indicates which term of equations (7) and (8) it is associated with. Magenta arrows represent the reflected field outside $\mathcal{R}$.
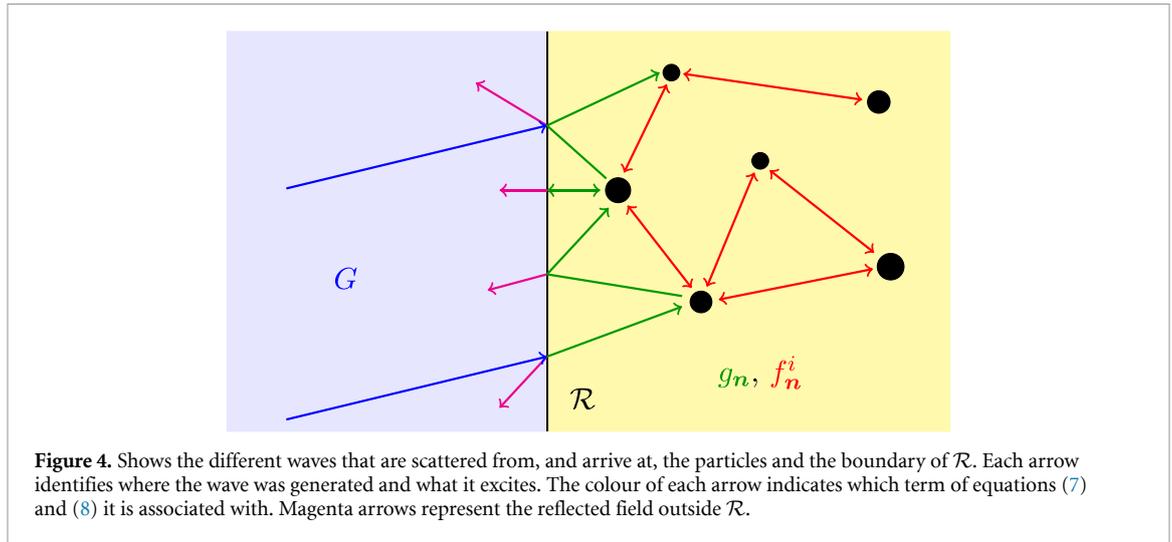
The total field in the exterior region equals the incident wave plus a reflected field,

$$u_{\text{tot}}(\boldsymbol{r}) = u_{\text{in}}(\boldsymbol{r}) + u_{\text{rf}}(\boldsymbol{r}) = G e^{i\boldsymbol{k}\cdot\boldsymbol{r}} + u_{\text{rf}}(\boldsymbol{r}), \quad \boldsymbol{r} \notin \mathcal{R} \tag{7}$$

where $G \in \mathbb{C}$ is the incident plane wave amplitude and $\boldsymbol{k} = (k_x, k_y, k_z)$ its wave vector, with $|\boldsymbol{k}| = k = \omega/c$ and $k_z > 0$. The reflected field u_{rf} is complicated and has no symmetry. We describe it in more detail in section 3.

3. One configuration of particles

Solving any wave scattering from one configuration of spheres in the matrix is a difficult problem [MS20, KW20], and as far as we know, there is no efficient semi-analytic solution for it. In this section, we formulate the basic equations for one configuration, which we use to study the ensemble average system.

We define the spherical solutions of the Helmholtz equation $u_{\boldsymbol{n}}$ and $v_{\boldsymbol{n}}$ (with $\boldsymbol{n} = (\ell, m)$, $\ell \in \mathbb{Z}_+$, $m = -\ell, \dots, \ell$), defined as

$$u_{\boldsymbol{n}}(k\boldsymbol{r}) = u_{(\ell,m)}(k\boldsymbol{r}) := h_\ell(kr)\,Y_{\boldsymbol{n}}(\hat{\boldsymbol{r}}),$$
$$v_{\boldsymbol{n}}(k\boldsymbol{r}) = v_{(\ell,m)}(k\boldsymbol{r}) := j_\ell(kr)\,Y_{\boldsymbol{n}}(\hat{\boldsymbol{r}}),$$

where (r, θ, ϕ) are the spherical coordinates of $\boldsymbol{r} \in \mathbb{R}^3$; $\hat{\boldsymbol{r}}$ is the unit vector in the direction of $\boldsymbol{r}$; $Y_{\boldsymbol{n}}(\hat{\boldsymbol{r}})$ are the spherical harmonic functions defined in appendix B; j_ℓ are spherical Bessel functions and h_ℓ are spherical Hankel functions, both of the first kind.

Within the matrix, and outside of the particles, the field can be written as a regular wave plus the waves scattered from each particle u_{sc}^i in the form[2]

$$u_{\text{tot}}(\boldsymbol{r}) = u_{\text{reg}}(\boldsymbol{r}) + \sum_{i=1}^{J} u_{\text{sc}}^i(\boldsymbol{r})$$

$$= \sum_{\boldsymbol{n}} g_{\boldsymbol{n}} v_{\boldsymbol{n}}(k_0 \boldsymbol{r}) + \sum_{i=1}^{J} \sum_{\boldsymbol{n}} f_{\boldsymbol{n}}^i u_{\boldsymbol{n}}(k_0 \boldsymbol{r} - k_0 \boldsymbol{r}_i), \quad \text{for} \quad \boldsymbol{r} \in \mathcal{R} \setminus \mathcal{P}, \tag{8}$$

where $\boldsymbol{r}_i$ is the position of the center of the i-th particle. The summations over the bold index $\boldsymbol{n}$ are performed as defined in appendix A. Figure 4 makes use of an arrow diagram to illustrate how waves scatter for one configuration of particles in the matrix.

Two types of waves contribute to regular field $u_{\text{reg}}(\boldsymbol{r})$: 1) the waves scattered between the boundary $\partial\mathcal{R}$ and the particles, and 2) the transmission of the incident field into the matrix. As $u_{\text{reg}}(\boldsymbol{r})$ contains no sources it is smooth in $\mathcal{R} \setminus \mathcal{P}$, and can therefore be expressed in terms of regular spherical waves.

We can use the boundary conditions on each of the particles to establish a relation between the coefficients $g_{\boldsymbol{n}}$ and $f_{\boldsymbol{n}}^i$. To achieve this, we define the field that excites the i-th particle $u_{\text{exc}}^i(\boldsymbol{r})$. This exciting wave is the sum of the waves scattered from all J particles different from the ith particle and the background

---

[2] The procedure to perform the summation over the double index $\boldsymbol{n} = (\ell, m)$ is given in appendix A.

regular field:

$$
\begin{aligned}
u_{\text{exc}}^{i}(\boldsymbol{r}) &:= u_{\text{reg}}(\boldsymbol{r}) + \sum_{\substack{j=1 \\ j \neq i}}^{J} u_{\text{sc}}^{j}(\boldsymbol{r}) \\
&= \sum_{\boldsymbol{n}} g_{\boldsymbol{n}} \mathrm{v}_{\boldsymbol{n}}(k_0 \boldsymbol{r}) + \sum_{\boldsymbol{n}} \sum_{j \neq i} f_{\boldsymbol{n}}^{j} \mathrm{u}_{\boldsymbol{n}}(k_0 \boldsymbol{r} - k_0 \boldsymbol{r}_j).
\end{aligned}
\tag{9}
$$

To apply the boundary conditions for particle i, we write (9) in a basis of spherical waves centred at $\boldsymbol{r}_i$ by using (60) which leads to

$$
u_{\text{exc}}^{i}(\boldsymbol{r}) = \sum_{\boldsymbol{n}\boldsymbol{n}'} \left[g_{\boldsymbol{n}} \mathcal{V}_{\boldsymbol{n}\boldsymbol{n}'}(k_0 \boldsymbol{r}_i) + \sum_{j \neq i} f_{\boldsymbol{n}}^{j} \mathcal{U}_{\boldsymbol{n}\boldsymbol{n}'}(k_0 \boldsymbol{r}_i - k_0 \boldsymbol{r}_j) \right] \mathrm{v}_{\boldsymbol{n}'}(k_0 \boldsymbol{r} - k_0 \boldsymbol{r}_i),
\tag{10}
$$

for $|\boldsymbol{r} - \boldsymbol{r}_i| < |\boldsymbol{r}_j - \boldsymbol{r}_i|$. Solving the boundary condition for particle i is now equivalent to applying the T-matrix [Wat71, VVP78, MTM96] $T_{\boldsymbol{n}}$ to the terms multiplying $\mathrm{v}_{\boldsymbol{n}'}(k_0 \boldsymbol{r} - k_0 \boldsymbol{r}_i)$ in (10), which leads to

$$
f_{\boldsymbol{n}}^{i} = T_{\boldsymbol{n}} \sum_{\boldsymbol{n}'} g_{\boldsymbol{n}'} \mathcal{V}_{\boldsymbol{n}'\boldsymbol{n}}(k \boldsymbol{r}_i) + T_{\boldsymbol{n}} \sum_{j \neq i} \sum_{\boldsymbol{n}'} f_{\boldsymbol{n}'}^{j} \mathcal{U}_{\boldsymbol{n}'\boldsymbol{n}}(k_0 \boldsymbol{r}_i - k_0 \boldsymbol{r}_j),
\tag{11}
$$

where the expression of the T-matrix for a homogeneous spherical particle is given by

$$
T_{\boldsymbol{n}} = T_{(\ell,m)} = -\frac{\gamma_{\text{s}} \mathrm{j}_{\ell}'(k_0 a) \mathrm{j}_{\ell}(k_{\text{s}} a) - \mathrm{j}_{\ell}(k_0 a) \mathrm{j}_{\ell}'(k_{\text{s}} a)}{\gamma_{\text{s}} \mathrm{h}_{\ell}'(k_0 a) \mathrm{j}_{\ell}(k_{\text{s}} a) - \mathrm{h}_{\ell}(k_0 a) \mathrm{j}_{\ell}'(k_{\text{s}} a)},
$$

with $\gamma_{\text{s}} := (\varrho_{\text{s}} c_{\text{s}})/(\varrho_0 c_0)$ and $k_{\text{s}} := \omega/c_{\text{s}}$.

The governing equation (11) is a straightforward generalisation of the case of particles in only one background medium. If the material properties of the matrix were the same as the exterior medium ($\varrho = \varrho_0$ and $c = c_0$), then $g_{\boldsymbol{n}}$ would represent the incident wave, as in [GK21, equation (2.7)].

Next, we need to establish a relation between the waves inside and outside the matrix; (11) and (7) respectively. Instead of directly using the boundary conditions (2), it is simpler to ensemble average the fields first. The averaging process will result in planar symmetry and simplify the form of (7) and (8), so that we can then apply the boundary condition at $z = 0$.

4. Ensemble averaging

One clear lesson from figure 4 is that $g_{\boldsymbol{n}}$ and $f_{\boldsymbol{n}}^{i}$ each depends on the positions of all the particles. Despite the rich number of interactions for one specific configuration, we show how the average field over all possible configurations can be simpler.

To reach the limit of an infinite number of particles, in a mathematically consistent way, we start with a cube $\mathcal{R}_{\eta}^{L}$ with a finite number of particles J. In set notation we have

$$
\mathcal{R}_{\eta}^{L} := \left\{ \boldsymbol{r}_i \in \mathbb{R}^3 \mid x_i \in (-L/2, L/2), \, y_i \in (-L/2, L/2), \, z_i \in (\eta, L + \eta) \right\},
\tag{12}
$$

where η is chosen later to create a space between the particles and the boundary, similar to section 1.1.

Now we can consider an ensemble for particles within $\mathcal{R}_{\eta}^{L}$. The probability density for the particles occupying the positions $\boldsymbol{r}_1, \boldsymbol{r}_2, \ldots, \boldsymbol{r}_J$ are given by

$$
p(\boldsymbol{r}_1, \boldsymbol{r}_2, \ldots, \boldsymbol{r}_J).
\tag{13}
$$

We define the ensemble average of any function f, which implicitly depends on the position and properties of the particles, over the configuration space as

$$
\langle \mathrm{f} \rangle := \int_{\left(\mathcal{R}_{\eta}^{L}\right)^{J}} \mathrm{f}\, p(\boldsymbol{r}_1, \boldsymbol{r}_2, \ldots, \boldsymbol{r}_J) \, \mathrm{d}\boldsymbol{r}_1 \mathrm{d}\boldsymbol{r}_2 \ldots \mathrm{d}\boldsymbol{r}_J,
\tag{14}
$$

where a set to the power J denotes the Cartesian product with itself J times. We also define the first and second conditional ensemble averages as

$$
\begin{aligned}
\langle \mathrm{f} \rangle(\boldsymbol{r}_1) &:= \int_{\left(\mathcal{R}_{\eta}^{L}\right)^{J-1}} \mathrm{f}\, p(\boldsymbol{r}_2, \ldots, \boldsymbol{r}_J | \boldsymbol{r}_1) \, \mathrm{d}\boldsymbol{r}_2 \ldots \mathrm{d}\boldsymbol{r}_J, \\
\langle \mathrm{f} \rangle(\boldsymbol{r}_1, \boldsymbol{r}_2) &:= \int_{\left(\mathcal{R}_{\eta}^{L}\right)^{J-2}} \mathrm{f}\, p(\boldsymbol{r}_3, \ldots, \boldsymbol{r}_J | \boldsymbol{r}_1, \boldsymbol{r}_2) \, \mathrm{d}\boldsymbol{r}_3 \ldots \mathrm{d}\boldsymbol{r}_J,
\end{aligned}
\tag{15}
$$

where we have used the marginalised probability functions for one and two particles, given by

$$p(\boldsymbol{r}_1) := \int_{\left(\mathcal{R}_\eta^L\right)^{J-1}} p(\boldsymbol{r}_1,\dots,\boldsymbol{r}_J) \; \mathrm{d}\boldsymbol{r}_2\dots\mathrm{d}\boldsymbol{r}_J,$$

$$p(\boldsymbol{r}_1,\boldsymbol{r}_2) := \int_{\left(\mathcal{R}_\eta^L\right)^{J-2}} p(\boldsymbol{r}_1,\dots,\boldsymbol{r}_J) \; \mathrm{d}\boldsymbol{r}_3\dots\mathrm{d}\boldsymbol{r}_J.$$

As in section 1.1, we assume particles are distributed homogeneously, which implies that

$$p(\boldsymbol{r}_i) = \frac{1}{L^3} = \frac{\mathfrak{n}}{J}, \quad \text{with} \quad \mathfrak{n} := \frac{J}{L^3}. \tag{16}$$

We call $\mathfrak{n}$ the particle number density.

For simplicity, we assume our particles are hard spheres (non-overlapping), and use the approximation known as hole correction:

$$p(\boldsymbol{r}_i|\boldsymbol{r}_j) = \begin{cases} p(\boldsymbol{r}_i)\dfrac{J}{J-1}, & \text{for } |\boldsymbol{r}_i - \boldsymbol{r}_j| > 2a, \\ 0, & \text{for } |\boldsymbol{r}_i - \boldsymbol{r}_j| \leqslant 2a, \end{cases} \tag{17}$$

where the factor $J/(J-1)$ comes from the fact that there are J particles within the cube $\mathcal{R}_\eta^L$. The need to add this extra factor in the case of a finite number of particles is explained in [Kon+04, equation (8.1.2)].

With our choice of pair correlation (17), and assuming the volume of $\mathcal{R}_\eta^L$ is much larger than the volume of the particles, we conclude that the position of just one of the particles does not significantly affect the probability distribution of the other particles. In other words, we assume

$$p(\boldsymbol{r}_2,\dots,\boldsymbol{r}_J|\boldsymbol{r}_1) \approx p(\boldsymbol{r}_2,\dots,\boldsymbol{r}_J), \tag{18}$$

$$p(\boldsymbol{r}_3,\dots,\boldsymbol{r}_J|\boldsymbol{r}_2,\boldsymbol{r}_1) \approx p(\boldsymbol{r}_3,\dots,\boldsymbol{r}_J|\boldsymbol{r}_2). \tag{19}$$

Another way of interpreting these approximations is by replacing conditional probabilities with its average over $\boldsymbol{r}_1$

$$p(\boldsymbol{r}_2,\dots,\boldsymbol{r}_J|\boldsymbol{r}_1) \approx \int_{\mathcal{R}_\eta^L} p(\boldsymbol{r}_2,\dots,\boldsymbol{r}_J|\boldsymbol{r}_1)p(\boldsymbol{r}_1)\,\mathrm{d}\boldsymbol{r}_1 = p(\boldsymbol{r}_2,\dots,\boldsymbol{r}_J),$$

$$p(\boldsymbol{r}_3,\dots,\boldsymbol{r}_J|\boldsymbol{r}_2,\boldsymbol{r}_1) \approx \int_{\mathcal{R}_\eta^L} p(\boldsymbol{r}_3,\dots,\boldsymbol{r}_J|\boldsymbol{r}_2,\boldsymbol{r}_1)p(\boldsymbol{r}_1|\boldsymbol{r}_2)\,\mathrm{d}\boldsymbol{r}_1 = p(\boldsymbol{r}_3,\dots,\boldsymbol{r}_J|\boldsymbol{r}_2).$$

5. Average fields

Our goal in this section is to describe the average scattered field close to the interface $z = 0$, so we can apply boundary conditions for the average total field. To make sure the particles do not touch the boundary at $z = 0$, as done in section 1.1, we take $\eta = a + \delta$ in (12), see figure 2(a). We remind the reader that a is the radius of the particles and $\delta/a \ll 1$ is a small parameter.

We start by computing the average of the total field. We multiply equation (7) by (13), use definition (14) for some fixed value of L, and then integrate over all possible particle positions to obtain

$$\langle u_{\text{tot}}(\boldsymbol{r})\rangle = G\mathrm{e}^{\mathrm{i}\boldsymbol{k}\cdot\boldsymbol{r}} + \langle u_{\text{rf}}(\boldsymbol{r})\rangle, \quad \text{for} \quad \boldsymbol{r} \notin \mathcal{R}. \tag{20}$$

Here we have $\langle G \rangle = G$ because the incident wave is the same for every configuration of particles. Computing the average of equation (8) results in

$$\langle u_{\text{tot}}(\boldsymbol{r})\rangle = \langle u_{\text{reg}}(\boldsymbol{r})\rangle + \sum_{j=1}^{J}\langle u_{\text{sc}}^j(\boldsymbol{r})\rangle,$$

where

$$\langle u_{\text{reg}}(\boldsymbol{r})\rangle = \sum_{\boldsymbol{n}}\langle g_{\boldsymbol{n}}\rangle \mathrm{v}_{\boldsymbol{n}}(k_0\boldsymbol{r}), \quad \text{for} \quad \boldsymbol{r} \in \mathcal{R}, \tag{21}$$

$$\sum_{j=1}^{J}\langle u_{\text{sc}}^j(\boldsymbol{r})\rangle = \sum_{i=1}^{J}\sum_{\boldsymbol{n}}\int_{\mathcal{R}_{a+\delta}^L}\langle f_{\boldsymbol{n}}^i\rangle(\boldsymbol{r}_i)\mathrm{u}_{\boldsymbol{n}}(k_0\boldsymbol{r} - k_0\boldsymbol{r}_i)p(\boldsymbol{r}_i)\,\mathrm{d}\boldsymbol{r}_i, \tag{22}$$

and (22) is valid for $0 \leqslant z \leqslant \delta$. This is because if $z > \delta$, then $\boldsymbol{r}$ could be inside a particle, in which case (8) would not be valid. In (22), $\langle f_{\boldsymbol{n}}^i \rangle (\boldsymbol{r}_i)$ is the average of $f_{\boldsymbol{n}}^i$ conditional to $\boldsymbol{r}_i$ as defined in (15)$_1$.

In our problem particles are indistinguishable, which enables us to use the simpler notation:

$$\langle f_{\boldsymbol{n}} \rangle (\boldsymbol{r}_i) := \langle f_{\boldsymbol{n}}^i \rangle (\boldsymbol{r}_i), \tag{23}$$

for $i = 1, 2, \ldots, J$. This notation makes it clear how to simplify the sums over particle indices. For example, substituting (16) and (23) into (22), leads to

$$\sum_{i=1}^{J} \langle u_{\text{sc}}^i (\boldsymbol{r}) \rangle = \mathfrak{n} \sum_{\boldsymbol{n}} \int_{\mathcal{R}_{a+\delta}^L} \langle f_{\boldsymbol{n}} \rangle (\boldsymbol{r}_1) \, \mathrm{u}_{\boldsymbol{n}} (k_0 \boldsymbol{r} - k_0 \boldsymbol{r}_1) \, \mathrm{d} \boldsymbol{r}_1. \tag{24}$$

5.1. The infinite volume limit

We now take the limit of $L \to \infty$ so that $\mathcal{R}_{a+\delta}^L$ becomes a halfspace, and compute the ensemble average for each term of the total average field, inside and outside the matrix.

Average regular field. Because we assume particles are uniformly distributed, see equation (16), and due to planar symmetry of the problem, the regular field evaluated in $z > 0$, shown in (21), can be represented as a plane wave after averaging:

$$\lim_{L \to \infty} \langle u_{\text{reg}} (\boldsymbol{r}) \rangle = \langle A \rangle \mathrm{e}^{\mathrm{i} \boldsymbol{k}_0 \cdot \boldsymbol{r}} + \langle A_- \rangle \mathrm{e}^{\mathrm{i} \boldsymbol{k}_0^- \cdot \boldsymbol{r}}, \quad \text{for} \quad z \geqslant 0,$$

where $\boldsymbol{k}_0 = (k_{0x}, k_{0y}, k_{0z}) := \left(k_x, k_y, \sqrt{k_0^2 - k_x^2 - k_y^2} \right)$ and $\boldsymbol{k}_0^- := (k_{0x}, k_{0y}, -k_{0z})$ are the wavevectors[3] of the plane waves. Without loss of generality, we choose $\mathrm{Im}[k_{0z}] \geqslant 0$ which implies that $\langle A_- \rangle = 0$ to avoid an unphysical wave. This choice also allows us to represent (21) in terms of a single plane wave, given by

$$\lim_{L \to \infty} \langle u_{\text{reg}} (\boldsymbol{r}) \rangle = \langle A \rangle \mathrm{e}^{\mathrm{i} \boldsymbol{k}_0 \cdot \boldsymbol{r}}. \tag{25}$$

The explicit expression for $\langle A \rangle$ in terms of $\langle g_{\boldsymbol{n}} \rangle$ is given in appendix B.

Average backscattered field. Taking the limit of $L \to \infty$ for the average backscattered field (24) leads to

$$\lim_{\substack{J \to \infty \\ L \to \infty}} \sum_{i=1}^{J} \langle u_{\text{sc}}^i (\boldsymbol{r}) \rangle = \mathfrak{n} \sum_{\boldsymbol{n}} \int_{\mathcal{R}_{a+\delta}} \langle f_{\boldsymbol{n}} \rangle (\boldsymbol{r}_1) \, \mathrm{u}_{\boldsymbol{n}} (k_0 \boldsymbol{r} - k_0 \boldsymbol{r}_1) \, \mathrm{d} \boldsymbol{r}_1, \tag{26}$$

where $\mathcal{R}_{a+\delta} := \lim_{L \to \infty} \mathcal{R}_{a+\delta}^L$ is the halfspace $z \geqslant a + \delta$. When taking this limit we need to fix the particle number density $\mathfrak{n}$, given in (16)$_2$, which implies that $J \to \infty$ when $L \to \infty$.

Less obviously, (26) also has a plane wave representation due to symmetry. In appendix C, D we show how to rewrite (26) as

$$\lim_{L \to \infty} \sum_{i=1}^{\infty} \langle u_{\text{sc}}^i (\boldsymbol{r}) \rangle = \langle B \rangle \mathrm{e}^{\mathrm{i} \boldsymbol{k}_0^- \cdot \boldsymbol{r}}, \quad \text{for} \quad 0 \leqslant z \leqslant \delta, \tag{27}$$

where the average backscattering amplitude $\langle B \rangle$ is given by

$$\langle B \rangle := \frac{2 \pi \mathfrak{n}}{k_0 k_{0z}} \sum_{\boldsymbol{n}} \mathrm{i}^{\ell} \mathrm{Y}_{\boldsymbol{n}} \left(\hat{\boldsymbol{k}}_0 \right) \int_{a+\delta}^{\infty} \langle f_{\boldsymbol{n}} \rangle (0, 0, z_1) \, \mathrm{e}^{\mathrm{i} k_{0z} z_1} \, \mathrm{d} z_1. \tag{28}$$

Average external field. By the same symmetry arguments, we know that the waves outside $\mathcal{R}$ can also be represented in terms of plane waves[3]:

$$\langle u_{\text{tot}} (\boldsymbol{r}) \rangle = G \mathrm{e}^{\mathrm{i} \boldsymbol{k} \cdot \boldsymbol{r}} + \langle R \rangle \mathrm{e}^{\mathrm{i} \left(k_x x + k_y y - k_z z \right)}, \quad \text{for} \quad z \leqslant 0 \tag{29}$$

where $\langle R \rangle$ is the average reflection amplitude. In section 5.2, we will derive a system of equations relating the amplitudes of the different fields. This will enable us to deduce $\langle R \rangle$, which is the quantity of main interest in this paper.

---

[3] Here we have used Snell's law to determine the components of the wavevectors for simplicity of the equations. However, this can be deduced directly from the transmission boundary conditions (30) in section 5.2 ahead.

5.2. Boundary conditions at the interface

To write down relations between the average amplitudes $\langle A \rangle$, $\langle B \rangle$ and $\langle R \rangle$, we need to impose boundary conditions at $z = 0$. We are interested in the case of homogeneous background media, so we choose transmission boundary conditions, which reads

$$\begin{cases} \langle u_{\text{tot}}(\boldsymbol{r}) \rangle \text{ is continuous at } z = 0, \\ \dfrac{1}{\rho(\boldsymbol{r})} \dfrac{\partial \langle u_{\text{tot}}(\boldsymbol{r}) \rangle}{\partial z} \text{ is continuous at } z = 0, \end{cases} \tag{30}$$

where $\rho(\boldsymbol{r})$ is the density, which is a function of $\boldsymbol{r} \in \mathbb{R}^3$.

We substitute (25), (27) and (29) into $(30)_1$ at the boundary $\bar{\boldsymbol{r}} = (x, y, 0)$:

$$G \mathrm{e}^{\mathrm{i}\boldsymbol{k}\cdot\bar{\boldsymbol{r}}} + \langle R \rangle \mathrm{e}^{\mathrm{i}\boldsymbol{k}\cdot\bar{\boldsymbol{r}}} = \langle A \rangle \mathrm{e}^{\mathrm{i}\boldsymbol{k}_0\cdot\bar{\boldsymbol{r}}} + \langle B \rangle \mathrm{e}^{\mathrm{i}\boldsymbol{k}_0\cdot\bar{\boldsymbol{r}}}$$

Because $\boldsymbol{k} \cdot \bar{\boldsymbol{r}} = \boldsymbol{k}_0 \cdot \bar{\boldsymbol{r}} = k_x x + k_y y$, the above simplifies to

$$G + \langle R \rangle = \langle A \rangle + \langle B \rangle. \tag{31}$$

Similar computations can be done as above, starting from $(30)_2$ instead of $(30)_1$. These result in another relation,

$$\frac{k_z}{\varrho}(G - \langle R \rangle) = \frac{k_{0z}}{\varrho_0}(\langle A \rangle - \langle B \rangle). \tag{32}$$

The system of equations (31) and (32) can be rearranged into

$$\langle R \rangle = \zeta_R G + \zeta_T \langle B \rangle, \quad \langle A \rangle = \gamma_0 \zeta_T G - \zeta_R \langle B \rangle, \tag{33}$$

where the newly introduced parameters ζ_R, ζ_T, γ_0 are given by

$$\zeta_R := \frac{\varrho_0 k_z - \varrho k_{0z}}{\varrho_0 k_z + \varrho k_{0z}}, \quad \zeta_T := \frac{2\varrho k_{0z}}{\varrho_0 k_z + \varrho k_{0z}}, \quad \gamma_0 := \frac{\varrho_0 k_z}{\varrho k_{0z}}.$$

At this point, we have three unknowns $\langle A \rangle$, $\langle B \rangle$, and $\langle R \rangle$ and two equations (33). The missing equation, which will be deduced in section 6, is determined by how the particles reflect waves in the region $\mathcal{R}$.

5.3. Single medium limit

As a sanity check, we can see how the equations (28) and (33) recover the single background medium limit. Taking the acoustic properties of the exterior medium and the matrix as the same ($c_0 = c$ and $\varrho_0 = \varrho$), we have that $\boldsymbol{k}_0 = \boldsymbol{k}$, which means $\zeta_R = 0$ and $\zeta_T = \gamma_0 = 1$. Substituting these values in (33) provides us with

$$\langle A \rangle = G, \quad \langle R \rangle = \langle B \rangle = \frac{2\pi \mathfrak{n}}{k k_z} \sum_{\boldsymbol{n}} \mathrm{i}^{\ell} \mathrm{Y}_{\boldsymbol{n}}\left(\hat{\boldsymbol{k}}\right) \int_a^{\infty} \langle f_{\boldsymbol{n}} \rangle (z_1) \, \mathrm{e}^{\mathrm{i}k z_1} \mathrm{d}z_1,$$

where we used (28) and took the limit $\delta \to 0$ to recover the formulas for particles distributed in a halfspace region $\mathcal{R}$, see figure 2(b). The above is the same formula for reflection of a halfspace as [GK21, equation (7.6)]. This means the approach is consistent with the average response of random particulate materials in the case of particles embedded in only one homogeneous medium.

6. Average backscattering operator

To obtain the final equation needed to determine the average amplitudes in (33), we follow the notation introduced in section 1.1. That is, we need to find an equation relating $\langle B \rangle$ and $\langle A \rangle$ through some backscattering operator $\langle \mathbb{T}_\sigma \rangle$. This final equation comes from the microstructure, which in our case is the ensemble averaged version of the boundary conditions of the particles (11).

Following the strategy of [GK21], we take a conditional ensemble average of (11), and use assumptions (16), (17), (23) to obtain

$$\langle f_{\boldsymbol{n}} \rangle (\boldsymbol{r}_1) = T_{\boldsymbol{n}} \sum_{\boldsymbol{n}'} \langle g_{\boldsymbol{n}'} \rangle (\boldsymbol{r}_1) \mathcal{V}_{\boldsymbol{n}'\boldsymbol{n}}(k_0 \boldsymbol{r}_1) + \mathfrak{n} T_{\boldsymbol{n}} \sum_{\boldsymbol{n}'} \int_{\mathcal{R}_a \backslash \mathcal{B}(\boldsymbol{r}_1, 2a)} \mathcal{U}_{\boldsymbol{n}'\boldsymbol{n}}(k_0 \boldsymbol{r}_1 - k_0 \boldsymbol{r}_2) \langle f_{\boldsymbol{n}'} \rangle (\boldsymbol{r}_2) \, \mathrm{d}\boldsymbol{r}_2 \tag{34}$$

where we used the standard QCA to substitute $\langle f_{\boldsymbol{n}} \rangle(\boldsymbol{r}_2, \boldsymbol{r}_1) = \langle f_{\boldsymbol{n}} \rangle(\boldsymbol{r}_2)$ [GK21].

By assuming that (34) has a unique solution for $\langle f_n \rangle (r_1)$ given $\langle g_{n'} \rangle (r_1)$, then, formally, we can use (34) to represent $\langle f_n \rangle (r_1)$ as

$$\langle f_n \rangle (r_1) = \sum_{n'} \mathcal{L}^f_{nn'} [\langle g_{n'} \rangle (r'_1)], \tag{35}$$

for some linear operator $\mathcal{L}^f_{nn'}$ acting on $\langle g_{n'} \rangle (r'_1)$. This operator notation $\mathcal{L}^f_{nn'}$ will help to compute $\langle \mathbb{T}_\sigma \rangle$. From (28) we see that $\langle B \rangle$ is a linear map acting on $\langle f_n \rangle$. For convenience, let us also represent (28) in the form $\langle B \rangle = \sum_n \mathcal{L}^B_n [\langle f_n \rangle (r_1)]$. Substituting (35) into this representation leads to

$$\langle B \rangle = \sum_{nn'} \mathcal{L}^B_n \left[\mathcal{L}^f_{nn'} [\langle g_{n'} \rangle (r'_1)] \right]. \tag{36}$$

It is not obvious, but (36) is the same as (5). And, just like in section 1.1, when combining (36) with the boundary conditions (33), we still have too many unknowns, and a closure assumption is required. The closure assumption which is consistent with the standard QCA is given by

$$\begin{aligned} \langle f_n \rangle (r_2, r_1) &= \langle f_n \rangle (r_2), \\ \langle g_n \rangle (r_1) &= \langle g_n \rangle, \end{aligned} \quad \text{(X-QCA)} \tag{37}$$

where X-QCA stands for the eXtended QCA. Below we show how this matches the closure assumption (6) in the introduction. In section 7 we deduce X-QCA from first principles, and show why it is the consistent way to extend QCA.

Substituting $(37)_2$ into (36), and using (63), leads to

$$\langle B \rangle = \langle \mathbb{T}_\sigma \rangle \langle A \rangle, \quad \text{with} \quad \langle \mathbb{T}_\sigma \rangle \equiv \sum_{nn'} \mathcal{L}^B_n \left[\mathcal{L}^f_{nn'} [C_{n'}] \right],$$

where the coefficients $C_{n'}$ are known quantities defined in appendix B. We clearly see now how the above is equivalent to approximation (6) in section 1.1.

With the above, together with (33), we can now calculate the solution, with an efficient numerical scheme shown in section 8, where we use the Effective Waves Method. To summarise, we can now obtain a governing equation for the unknowns by substituting (36) into (34), and using (63) from appendix B, leading to:

$$\langle f_n \rangle (r_1) = \langle A \rangle T_n \sum_{n'} C_{n'} \mathcal{V}_{n'n} (k_0 r_1) + \mathfrak{n} T_n \sum_{n'} \int_{\mathcal{R}_a \backslash \mathcal{B}(r_1, 2a)} \mathcal{U}_{n'n} (k_0 r_1 - k_0 r_2) \langle f_{n'} \rangle (r_2) \, dr_2. \tag{38}$$

We could now, in theory, numerically solve for $\langle f_n \rangle (r_1)$, $\langle A \rangle$, $\langle B \rangle$, and $\langle R \rangle$, by combining (38) with the boundary conditions (33) and the definition of $\langle B \rangle$ in terms of the $\langle f_n \rangle (r_1)$ given by (28). However, we present a far more efficient method to solve this in section 8.

6.1. The average reflection coefficient

With all the computations so far we have successfully deduced the contribution to sound wave scattering due to particles (38) and the halfspace interface (33) as two separate equations, as briefed in section 1.1. Then, we substitute $(33)_{(2)}$ into (38) to compute a single integral equation in $\langle f_n \rangle (r_1)$, which reads

$$\langle f_n \rangle (r_1) = \gamma_0 \zeta_T T_n W_n (r_1) G + T_n D_n (r_1) [\langle f_{n'} \rangle] - \zeta_R T_n W_n (r_1) \langle B \rangle [\langle f_{n'} \rangle], \tag{39}$$

where we have defined the particle-rescattering operator

$$D_n (r) [\langle f_{n'} \rangle] := \mathfrak{n} \sum_{n'} \int_{\mathcal{R}_a \backslash \mathcal{B}(r, 2a)} \mathcal{U}_{n'n} (k_0 r - k_0 r') \langle f_{n'} \rangle (r') \, dr'.$$

and the interface coupling function

$$W_n (r_1) := \sum_{n'} C_{n'} \mathcal{V}_{n'n} (k_0 r_1) = C_n e^{i k_0 \cdot r_1}, \tag{40}$$

where we used [GK21, eqs. (A.2) and (B.12)] to write the second equality in (40).

If the geometry of the matrix containing the particles is changed, the same equation (39) can still be used, however, the terms involving the interface coupling factor (40) will change. Also, the explicit equation for the boundary conditions (33) will not be the same.

As we shall see further on, equation (39) is enough to determine $\langle f_{\boldsymbol{n}} \rangle (\boldsymbol{r}_1)$, making it possible to compute the expression of the total wave outside the halfspace $\mathcal{R}$. We recall the expression for the reflection coefficient (33)$_{(1)}$ below:

$$\langle R \rangle = \zeta_R \, G + \zeta_T \, \langle B \rangle.$$

The first term is the reflection coefficient from a homogeneous matrix without any particles inside. Only the second term $\zeta_T \langle B \rangle$ carries the effects of scattering from the particles. In others words, if we knew the background material, and wanted to use a reflection experiment to characterise the particles, then we should use the expression $\langle R \rangle - \zeta_R \, G$ to do so.

There have been many uses of reflection coefficients from particulates in the literature, see for example [Gar+05, CPS11, Sim+24]. In [Sim+24] they used approximate formulas for the reflection coefficient (33)$_{(1)}$ and obtained a good qualitative agreement with experimental data [Sim+24]. Having the exact formula (33)$_{(1)}$, calculated from first principles, would likely lead to more accurate predictions, especially for a broad frequency range, which is less understood.

7. Extended QCA

In this section, we explain why the eXtended Quasi-Crystalline Approximation (X-QCA) (37) is accurate, for low and high volume fraction of particles, and show that it is the systematic extension of the standard QCA [Lax52] to scenarios with different background mediums.

To justify X-QCA (37) it is best to start with just one configuration of particles, as this will help us understand the role of the different waves.

We recall from figure 4 that the field (9) which excites particle i depends on the configuration of all particles, including its own position $\boldsymbol{r}_i$. Take, for example, any wave which is initially scattered from particle i and then returns to particle i due to multiple scattering. This type of dependence is called self-interaction, and it is known in the statistical mechanics literature that accounting for self-interactions can lead to unsolvable equations, or even divergences, when ensemble averaging [HBE87, DM18]. This is the case for any particulate material, whether there are different background mediums or not.

For clarity, let us introduce the notation:

$$u_{\mathrm{exc}}^1 (\boldsymbol{r}; \boldsymbol{r}_1, \boldsymbol{r}_2, \ldots, \boldsymbol{r}_J) := u_{\mathrm{exc}}^1 (\boldsymbol{r}),$$

to denote the exciting field u_{exc}^1, so that we can explicitly discuss how u_{exc}^1 depends on the positions $\boldsymbol{r}_j$ of each particle.

A possible strategy to simplify the self-interactions is to approximate the field exciting particle 1, for example, by its own conditional average:

$$u_{\mathrm{exc}}^1 (\boldsymbol{r}; \boldsymbol{r}_1, \boldsymbol{r}_2, \ldots, \boldsymbol{r}_J) \approx \langle u_{\mathrm{exc}}^1 \rangle_1 (\boldsymbol{r}; \boldsymbol{r}_2, \ldots, \boldsymbol{r}_J) \tag{41}$$

where we used the conditional average:

$$\langle u_{\mathrm{exc}}^1 \rangle_1 (\boldsymbol{r}; \boldsymbol{r}_2, \ldots, \boldsymbol{r}_J) := \int_{\mathcal{R}_{a+\delta}^L} u_{\mathrm{exc}}^1 (\boldsymbol{r}; \boldsymbol{r}_1', \boldsymbol{r}_2, \ldots, \boldsymbol{r}_J) \, p \, (\boldsymbol{r}_1' | \boldsymbol{r}_2, \ldots, \boldsymbol{r}_J) \, \mathrm{d}\boldsymbol{r}_1'. \tag{42}$$

We will show how (41) leads to the standard QCA [Lax52] when there is just one background medium, and it also leads to X-QCA when there are different background mediums and interfaces. But first, let us consider whether it is a sensible approximation.

Is the approximation (41) accurate? figure 5 illustrates some of the possible positions $\boldsymbol{r}_1'$ of the first particle, and how they contribute to the field exciting the particle positioned at $\boldsymbol{r}_1$. We will explain why (41) is highly accurate for large and small particle volume fractions. We note that similar arguments have been used in [WT61, FW64, MVV84].

For a small volume fraction of particles, the wave scattered from particle i will be weakly rescattered by the same particle i, as the average distances to the next particle, or interface, are large. In which case $u_{\mathrm{exc}}^1 (\boldsymbol{r}; \boldsymbol{r}_1, \boldsymbol{r}_2, \ldots)$ weakly depends on the position of particle 1. From this we can deduce the approximation (41) by taking $u_{\mathrm{exc}}^1 (\boldsymbol{r}; \boldsymbol{r}_1, \boldsymbol{r}_2, \ldots)$ out of the integral in (42) together with

$$\int_{\mathcal{R}_{a+\delta}^L} p \, (\boldsymbol{r}_1' | \boldsymbol{r}_2 \ldots, \boldsymbol{r}_J) \, \mathrm{d}\boldsymbol{r}_1' = 1.$$
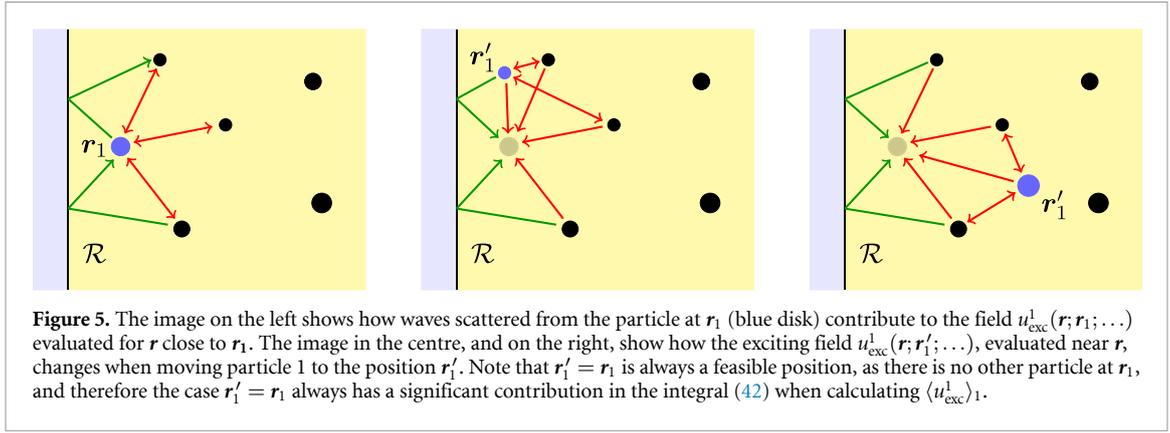
Figure 5. The image on the left shows how waves scattered from the particle at r_1 (blue disk) contribute to the field $u^1_{exc}(r; r_1; \ldots)$ evaluated for r close to r_1. The image in the centre, and on the right, show how the exciting field $u^1_{exc}(r; r'_1; \ldots)$, evaluated near r, changes when moving particle 1 to the position r'_1. Note that $r'_1 = r_1$ is always a feasible position, as there is no other particle at r_1, and therefore the case $r'_1 = r_1$ always has a significant contribution in the integral (42) when calculating $\langle u^1_{exc} \rangle_1$.

For a large volume fraction of particles, most of all particle positions r'_1 in the integral (42) would be prohibitive, as the particles are densely packed together and particles can not overlap. That is, the function $p(r'_1 | r_2 \ldots, r_J)$ is zero when particles overlap. This is illustrated in figure 5. The one region that most contributes to the integral in (42) is the region around the original particle position r_1. An extreme example of this is a crystal, where the neighbouring particles exactly determine the position of r'_1 and

$$p(r'_1 | r_2, \ldots, r_J) = \delta(r'_1 - r_1),$$

which substituted into (41) leads to $u^1_{exc}(r; r_1, r_2 \ldots) = \langle u^1_{exc} \rangle_1 (r; r_2, \ldots)$ exactly.

The discussion above shows why (41) is a good approximation, which justifies why it is commonly used in the literature [MVV84, TPM11, LM05, GPA19, KW20, KPG24, NPG24]. In section 7.1 we show how approximation (41) leads to X-QCA (37), and therefore is equivalent to standard QCA when there is just one background medium.

7.1. The average exciting field
To reach X-QCA (37) (or the standard QCA) from the approximation (41) we start with definition (9), rename r_1 to r'_1, multiply both sides by $p(r'_1 | r_2, \ldots, r_J)$, integrate over r'_1, and then use (42) together with the approximation (41) to arrive at

$$u^1_{exc}(r) = \sum_n \langle g_n \rangle_1 v_n(k_0 r) + \sum_n \sum_{j=2}^{J} \langle f^j_n \rangle_1 u_n(k_0 r - k_0 r_j). \tag{43}$$

Note, in practice the only difference between (43) and (9) is that we have replaced g_n by $\langle g_n \rangle_1$ and f^j_n by $\langle f^j_n \rangle_1$ for $j \neq 1$.

Following the same steps as done in sections 5 and 6, we would obtain the same expression as in (34), except with the substitutions

$$\langle g_n \rangle(r_1) = \langle \langle g_n \rangle_1 \rangle(r_1) \quad \text{and} \quad \langle f_n \rangle(r_2, r_1) = \langle \langle f_n \rangle_1 \rangle(r_2, r_1),$$

we show below that these are equivalent to (37) for disordered particulates. Combining the definition (42) (with g_n in place of u^1_{exc}) with the definition (15) leads to

$$
\begin{aligned}
\langle \langle g_n \rangle_1 \rangle(r_1) &= \int g_n p(r'_1 | r_2, \ldots) p(r_2, \ldots | r_1) \, dr'_1 dr_2 \ldots dr_J \\
&= \int g_n \frac{p(r'_1, r_2, \ldots)}{p(r_2, r_3, \ldots)} p(r_2, r_3, \ldots | r_1) \, dr'_1 dr_2 \ldots dr_J \\
&= \int g_n p(r'_1, r_2, \ldots) \, dr'_1 \ldots dr_J = \langle g_n \rangle,
\end{aligned}
\tag{44}
$$

where in the third line we used assumption (18), which is valid for a large number of disordered particles. Similarly, we have that

$$
\begin{aligned}
\langle \langle f_{\boldsymbol{n}'}^2 \rangle_1 \rangle (\boldsymbol{r}_2, \boldsymbol{r}_1) &= \int f_{\boldsymbol{n}'}^2 p\left(\boldsymbol{r}_1' | \boldsymbol{r}_2, \dots\right) p\left(\boldsymbol{r}_3, \dots | \boldsymbol{r}_2, \boldsymbol{r}_1\right) \mathrm{d}\boldsymbol{r}_1' \mathrm{d}\boldsymbol{r}_3 \dots \mathrm{d}\boldsymbol{r}_J \\
&= \int f_{\boldsymbol{n}'}^2 \frac{p\left(\boldsymbol{r}_1', \dots\right)}{p\left(\boldsymbol{r}_2, \dots\right)} p\left(\boldsymbol{r}_3, \dots | \boldsymbol{r}_2, \boldsymbol{r}_1\right) \mathrm{d}\boldsymbol{r}_1' \mathrm{d}\boldsymbol{r}_3 \dots \mathrm{d}\boldsymbol{r}_J \\
&= \int f_{\boldsymbol{n}'}^2 \frac{p\left(\boldsymbol{r}_1', \boldsymbol{r}_3, \dots | \boldsymbol{r}_2\right)}{p\left(\boldsymbol{r}_3, \dots | \boldsymbol{r}_2\right)} p\left(\boldsymbol{r}_3, \dots | \boldsymbol{r}_2, \boldsymbol{r}_1\right) \mathrm{d}\boldsymbol{r}_1' \mathrm{d}\boldsymbol{r}_3 \dots \mathrm{d}\boldsymbol{r}_J \\
&= \int f_{\boldsymbol{n}'}^2 p\left(\boldsymbol{r}_1', \boldsymbol{r}_3, \dots | \boldsymbol{r}_2\right) \mathrm{d}\boldsymbol{r}_1' \mathrm{d}\boldsymbol{r}_3 \dots \mathrm{d}\boldsymbol{r}_J \\
&= \langle f_{\boldsymbol{n}'}^2 \rangle (\boldsymbol{r}_2) = \langle f_{\boldsymbol{n}'} \rangle (\boldsymbol{r}_2),
\end{aligned}
\tag{45}
$$

where we repeatedly used the definition of conditional probability, and to reach the fourth line we used assumption (19).

The results in (44) and (45) demonstrate that approximation (37) is a consequence of approximation (41) for disordered particulates as defined in section 4. Because the approximation holds for any number of particles and any size of $|\mathcal{R}_{a+\delta}^L|$, (37) is valid for the limit of infinite particles defined in section 5.1.

An advantage of using approximations in terms of the exciting field (41), instead of quantities which are more directly related to the particles, such as (37), is that it is clear how to extend this approximation to more complex scenarios. In the presence of other geometries, layers, or multispecies [Gow+18], we can still define an exciting field, and then use (41) directly. It is also possible to account for more complex interactions between particles other than the pair correlation (17) assumed in this work. See [Twe64, TPM11] for a broader discussion on how to account for different pair correlations for standard QCA. In other words, approximation (41) leads to a systematic way to generalise the original QCA introduced in [Lax52].

Beyond generalising QCA, we feel that approximation (41) provides more physical insight. We saw from the section 7 that QCA, and its extension, only approximate the self-interaction by averaging it (conditioned on the position of the other particles). This has already been discussed for the classical QCA through a scattering series expansion [TPM11]. As a consequence, QCA, and its extension, is only making an approximation about third-order and higher scattering[4]. This sheds light on the agreement between second-order weak scattering approximations and QCA, as discussed in [MM08].

Finally, we note that some work has been carried out in the literature [KW20] which was able to write down a closed system of equations by using the classical QCA, but without making an approximation on the regular field $\langle g_{\boldsymbol{n}} \rangle (\boldsymbol{r}_1)$. However, when using QCA, we would already be making an approximation about third-order scattering, so there is no reason to retain high-order scattering for some terms (from a wall) but not from others (particles). Further, X-QCA leads to systems which are far simpler to solve, as we demonstrate in section 8.

8. Effective waves method

We use the Effective Waves Method, introduced in [GK21], to solve the governing equation (39). As shown in [GK21], it is usually accurate, even for a broad range of frequencies and particle volume fractions[5] to assume that $\langle f_{\boldsymbol{n}} \rangle$ satisfies the 3D Helmholtz equation with the effective wavenumber k_*

$$
\nabla^2 \langle f_{\boldsymbol{n}} \rangle (\boldsymbol{r}_1) + k_*^2 \langle f_{\boldsymbol{n}} \rangle (\boldsymbol{r}_1) = 0 \quad \text{for} \quad \boldsymbol{r}_1 \in \mathcal{R}_a.
\tag{46}
$$

Then, by using plane wave symmetry, shown in appendix C with (65), we conclude that

$$
\langle f_{\boldsymbol{n}} \rangle (\boldsymbol{r}_1) = F_{\boldsymbol{n}} \mathrm{e}^{\mathrm{i} \boldsymbol{k}_* \cdot \boldsymbol{r}_1},
\tag{47}
$$

where $\boldsymbol{k}_* = (k_{*x}, k_{*y}, k_{*z}) := \left(k_x, k_y, \sqrt{k_*^2 - k_x^2 - k_z^2} \right)$. We also choose $\mathrm{Im}[k_{*z}] \geqslant 0$, similarly to (25) in section 5.1.

---

[4] An example of third-order self-interaction scattering would be: the incident wave scatters on the *i*-th particle, which then gets scattered by the *j*-th particle, and finally reaches the *i*-th particle again, scattering once more. See figure 3 in [TPM11] for the Feynman diagrams.
[5] The general solution presented in [GK21] introduces multiple wavenumbers, although they argue that there is usually only one dominant wavenumber k_* for most properties and frequencies. See [KPG24] for phase diagrams that show when more than one wavenumber is needed.

Now, we take the limit $\delta \to 0$ to represent the case of a halfspace $\mathcal{R}$ filled with particles, as illustrated in figure 2(b). We also define the bulk region as done in [GHK23]:

$$\mathcal{R}_{\text{Bulk}} := \left\{ \boldsymbol{r}_1 \in \mathbb{R}^3 | z_1 > 2a \right\}. \tag{48}$$

Below we follow the steps shown in [GHK23] to deduce an effective wave equation and ensemble boundary conditions. We need to redo the steps here, as having a different background medium for the matrix does lead to some important differences.

To start we note that

$$\left(k_0^2 - k_*^2 \right) \mathcal{U}_{\boldsymbol{n}'\boldsymbol{n}} \left(k\boldsymbol{r}_1 - k\boldsymbol{r}_2 \right) \langle f_{\boldsymbol{n}'} \rangle \left(\boldsymbol{r}_2 \right)$$
$$= \mathcal{U}_{\boldsymbol{n}'\boldsymbol{n}} \left(k_0\boldsymbol{r}_1 - k_0\boldsymbol{r}_2 \right) \nabla_{\boldsymbol{r}_2}^2 \langle f_{\boldsymbol{n}'} \rangle \left(\boldsymbol{r}_2 \right) - \langle f_{\boldsymbol{n}'} \rangle \left(\boldsymbol{r}_2 \right) \nabla_{\boldsymbol{r}_2}^2 \mathcal{U}_{\boldsymbol{n}'\boldsymbol{n}} \left(k_0\boldsymbol{r}_1 - k_0\boldsymbol{r}_2 \right), \tag{49}$$

for $\boldsymbol{r}_1 \in \mathcal{R}_{\text{Bulk}}$ and $\boldsymbol{r}_2 \in \mathcal{R}_a$, because $\mathcal{U}_{\boldsymbol{n}'\boldsymbol{n}}(k\boldsymbol{r}_1 - k\boldsymbol{r}_2)$ and $\langle f_{\boldsymbol{n}'} \rangle(\boldsymbol{r}_2)$ satisfy Helmholtz equations with wavenumbers k_0 and k_* respectively. Then, by integrating the right side of (49) over $\boldsymbol{r}_2 \in \mathcal{R}_a \backslash \mathcal{B}(\boldsymbol{r}_1, 2a)$ and using Green's second identity, we get

$$\int_{\mathcal{R}_a \backslash \mathcal{B}(\boldsymbol{r}_1, 2a)} \mathcal{U}_{\boldsymbol{n}'\boldsymbol{n}} \left(k_0\boldsymbol{r}_1 - k_0\boldsymbol{r}_2 \right) \langle f_{\boldsymbol{n}'} \rangle \left(\boldsymbol{r}_2 \right) \mathrm{d}\boldsymbol{r}_2 \mathrm{d}\lambda = \frac{\mathcal{I}_{\boldsymbol{n}'\boldsymbol{n}}(\boldsymbol{r}_1) - \mathcal{J}_{\boldsymbol{n}'\boldsymbol{n}}(\boldsymbol{r}_1)}{\left(k_0^2 - k_*^2 \right)}, \tag{50}$$

where $\mathcal{I}_{\boldsymbol{n}'\boldsymbol{n}}(\boldsymbol{r})$ and $\mathcal{J}_{\boldsymbol{n}'\boldsymbol{n}}(\boldsymbol{r})$ are given by

$$\mathcal{I}_{\boldsymbol{n}'\boldsymbol{n}}(\boldsymbol{r}_1) := -F_{\boldsymbol{n}'} \int_{\partial\mathcal{R}_a} \mathcal{U}_{\boldsymbol{n}'\boldsymbol{n}} \left(k_0\boldsymbol{r}_1 - k_0\boldsymbol{r}_2 \right) \frac{\partial \mathrm{e}^{\mathrm{i}\boldsymbol{k}_* \cdot \boldsymbol{r}_2}}{\partial z_2} - \frac{\partial \mathcal{U}_{\boldsymbol{n}'\boldsymbol{n}} \left(k_0\boldsymbol{r}_1 - k_0\boldsymbol{r}_2 \right)}{\partial z_2} \mathrm{e}^{\mathrm{i}\boldsymbol{k}_* \cdot \boldsymbol{r}_2} \mathrm{d}S_2,$$

$$\mathcal{J}_{\boldsymbol{n}'\boldsymbol{n}}(\boldsymbol{r}_1) := F_{\boldsymbol{n}'} \int_{\partial\mathcal{B}(0,2a)} \mathcal{U}_{\boldsymbol{n}'\boldsymbol{n}} \left(-k_0\boldsymbol{r}' \right) \frac{\partial \mathrm{e}^{\mathrm{i}\boldsymbol{k}_* \cdot (\boldsymbol{r}' + \boldsymbol{r}_1)}}{\partial z} - \frac{\partial \mathcal{U}_{\boldsymbol{n}'\boldsymbol{n}} \left(-k_0\boldsymbol{r}' \right)}{\partial z} \mathrm{e}^{\mathrm{i}\boldsymbol{k}_* \cdot (\boldsymbol{r}' + \boldsymbol{r}_1)} \mathrm{d}S',$$

with $\mathrm{d}S_2$ and $\mathrm{d}S'$ being the area elements. Also, in the second line of the above, we have performed the change of coordinates $\boldsymbol{r}_2 \to \boldsymbol{r}' + \boldsymbol{r}_1$.

We substitute expression (50) into (39) to reach

$$\langle f_{\boldsymbol{n}} \rangle (\boldsymbol{r}_1) = T_{\boldsymbol{n}} W_{\boldsymbol{n}} (\boldsymbol{r}_1) \left(\gamma_0 \zeta_T G - \zeta_R \langle B \rangle \right) + \mathfrak{n} \frac{T_{\boldsymbol{n}}}{k_0^2 - k_*^2} \sum_{\boldsymbol{n}'} \left(\mathcal{I}_{\boldsymbol{n}'\boldsymbol{n}}(\boldsymbol{r}_1) - \mathcal{J}_{\boldsymbol{n}'\boldsymbol{n}}(\boldsymbol{r}_1) \right), \tag{51}$$

and we notice that $\langle f_{\boldsymbol{n}} \rangle (\boldsymbol{r}_1, \lambda)$ and $\mathcal{J}_{\boldsymbol{n}'\boldsymbol{n}}(\boldsymbol{r}_1)$ satisfy the Helmholtz equation with wavenumber k_*, while $W_{\boldsymbol{n}}(\boldsymbol{r}_1)$ and $\mathcal{I}_{\boldsymbol{n}'\boldsymbol{n}}(\boldsymbol{r}_1)$ satisfy the Helmholtz equation with wavenumber k_0. Because $k_0 \neq k_*$, see [GK21, appendix C], we can split (51) into

$$\langle f_{\boldsymbol{n}} \rangle (\boldsymbol{r}_1) + \mathfrak{n} \sum_{\boldsymbol{n}'} \frac{T_{\boldsymbol{n}}}{k_0^2 - k_*^2} \mathcal{J}_{\boldsymbol{n}'\boldsymbol{n}}(\boldsymbol{r}_1) = 0, \tag{52}$$

$$W_{\boldsymbol{n}}(\boldsymbol{r}_1) \left(\gamma_0 \zeta_T G - \zeta_R \langle B \rangle \right) + \frac{\mathfrak{n}}{k_0^2 - k_*^2} \sum_{\boldsymbol{n}'} \mathcal{I}_{\boldsymbol{n}'\boldsymbol{n}}(\boldsymbol{r}_1) = 0. \tag{53}$$

Equation (52) is called the ensemble wave equation, and it is identical to [GK21, eq. (4.7)], which is expected because (52) is fully determined by the microstructure of the particulate material and not the exterior medium.

Equation (53) is similar to the ensemble boundary conditions in [GK21, eq. 4.8]. However, (53) has one extra term representing the interaction between particles and the interface of the halfspace at $z = 0$.

Following the same steps as in [GK21], one can use (52) to write down the following eigensystem for the eigenpair $(k_*, F_{\boldsymbol{n}})$:

$$F_{\boldsymbol{n}} + 8\pi a T_{\boldsymbol{n}} \sum_{\boldsymbol{n}', \boldsymbol{n}_1} \frac{c_{\boldsymbol{n}'\boldsymbol{n}\boldsymbol{n}_1}}{k_*^2 - k_0^2} \mathrm{i}^{-\ell_1} \mathrm{Y}_{\boldsymbol{n}_1} \left(\hat{\boldsymbol{k}}_* \right) \mathrm{N}_{\ell_1} \left(2k_0 a, 2k_* a \right) \mathfrak{n} F_{\boldsymbol{n}'} = 0, \tag{54}$$

with $\boldsymbol{n}_1 = (\ell_1, m_1)$. The expression for $\mathrm{N}_\ell(x, z)$ and $c_{\boldsymbol{n}\boldsymbol{n}'\boldsymbol{n}_1}$ are defined in [GK21, eqs. (5.5) and (B.4) respectively].

8.1. Normalisation condition

The solution of (54) provides the effective wavenumber k_*, however the eigenvectors F_n are determined only up to a multiplicative factor. The ensemble boundary condition (53) is needed to find a normalisation condition for F_n, and fully determine the average field amplitude. To do so, we start by substituting (40) and [GK21, equation (7.10)] into (53), leading to

$$
C_n \mathrm{e}^{\mathrm{i} k_0 \cdot r_1} \left(\gamma_0 \zeta_T G - \zeta_R \langle B \rangle \right) = C_n \mathrm{e}^{\mathrm{i} k_0 \cdot r_1} \frac{\mathfrak{n}}{k_0^2 - k_*^2} \sum_{n'} \mathrm{K}_{n'}(a) F_{n'},
\tag{55}
$$

where we defined

$$
\mathrm{K}_{(\ell', m')}(a) := \frac{2\pi \mathrm{i}}{k_0 k_{0z}} \left(-\mathrm{i} \right)^{\ell'} \mathrm{Y}_{(\ell', m')}\left(\hat{k}_0 \right) \left(k_{*z} + k_{0z} \right) \mathrm{e}^{\mathrm{i}(k_{*z} - k_{0z})a}.
$$

Then, we substitute (47) into (28) to write down

$$
\langle B \rangle = -\frac{2\pi \mathfrak{n}}{k_0 k_{0z}} \frac{\mathrm{e}^{\mathrm{i}(k_{*z} + k_{0z})a}}{\mathrm{i}\left(k_{*z} + k_{0z} \right)} \sum_{(\ell, m)} \mathrm{i}^{\ell} \mathrm{Y}_{(\ell, m)}\left(\hat{k}_0 \right) F_{(\ell, m)},
\tag{56}
$$

and we remind the reader we have already taken the limit $\delta \to 0$ at the beginning of section 8.

Then, we substitute (56) into (55) and divide both sides by $C_n \mathrm{e}^{\mathrm{i} k_0 \cdot r_1}$ to obtain

$$
\gamma_0 \zeta_T G + \zeta_R \frac{2\pi \mathfrak{n}}{k_0 k_{0z}} \frac{\mathrm{e}^{\mathrm{i}(k_{*z} + k_{0z})a}}{\mathrm{i}\left(k_{*z} + k_{0z} \right)} \sum_{n'} \mathrm{i}^{\ell'} \mathrm{Y}_{n'}\left(\hat{k}_0 \right) F_{n'} = \frac{\mathfrak{n}}{k_0^2 - k_*^2} \sum_{n'} \mathrm{K}_{n'}(a) F_{n'},
$$

where $n' = (\ell', m')$.

Finally, we gather the terms which contain $F_{n'}$ on the left-hand side to write down the following normalisation condition:

$$
\sum_{n'} \mathrm{M}_{n'} F_{n'} = \gamma_0 \zeta_T G,
\tag{57}
$$

where

$$
\mathrm{M}_{(\ell', m')} := \frac{\mathfrak{n}}{k_0^2 - k_*^2} \mathrm{K}_{(\ell', m')}(a) - \zeta_R \frac{2\pi \mathfrak{n}}{k_0 k_{0z}} \frac{\mathrm{e}^{\mathrm{i}(k_{*z} + k_{0z})a}}{\left(k_{*z} + k_{0z} \right)} \mathrm{i}^{\ell' - 1} \mathrm{Y}_{(\ell', m')}\left(\hat{k}_0 \right).
$$

This normalisation condition is the last equation needed to numerically calculate the eigenvectors F_n, and together with k_*, they determine all the average amplitudes $\langle B \rangle$, $\langle R \rangle$ and $\langle A \rangle$ through equations (28) and (33) respectively.

8.2. High frequency limit

As a side quest, here we deduce that, in the high frequency limit, the average reflection coefficient $\langle R \rangle$ does not depend on the particle properties. In fact, $\langle R \rangle$ is just the reflection from the matrix itself without particles in this limit. Results for high frequency, such as this, are not very common or well understood in the literature.

We start by defining the volume fraction of particles as

$$
\phi := \frac{|\mathcal{P}|}{|\mathcal{R}_a|} = \frac{4\pi a^3}{3} \mathfrak{n}.
\tag{58}
$$

Substituting (58) into (56), one can deduce that

$$
\begin{aligned}
|\langle B \rangle| &= \frac{3}{2} \frac{\phi \, \mathrm{e}^{-\mathrm{Im}[k_{*z}]a}}{(k_0 a)(k_{0z} a)\,|k_{*z} + k_{0z}|a} \left| \sum_{(\ell, m)} \mathrm{i}^{\ell} \mathrm{Y}_{(\ell, m)}\left(\hat{k}_0 \right) F_{(\ell, m)} \right| \\
&\leqslant \frac{3}{2} \frac{\phi \, \mathrm{e}^{-\mathrm{Im}[k_{*z}]a}}{(k_0 a)(k_{0z} a)\,|k_{*z} + k_{0z}|a} \sum_n \left| \mathrm{Y}_n\left(\hat{k}_0 \right) \right| |F_n|,
\end{aligned}
\tag{59}
$$

which we will use to show that $|\langle B \rangle| \to 0$ when $ka \to \infty$.

Figure 6. Numerical computations of the average reflection coefficient $\langle R \rangle$ divided by the incident wave amplitude G by using the Effective Waves Method ('EW Method'). The particles are bubbles of gas in water ($c_s = c_0/100$, $\varrho_s = \varrho_0/100$) with volume fraction $\phi = 10\%$. The horizontal axis is the dimensionless frequency $k_0 a$ and θ is the angle of incidence. On the left, the plane wave incidence is normal ($k_x = k_y = 0$), while on the right the angle of incidence is varying ($k_x \geqslant 0$, $k_y = 0$). The dashed lines represent the low frequency limit response and the reflection without any particles in the matrix. The exterior medium is a solid ($c = 3c_0$, $\varrho = 3\varrho_0$). See [Pau24] for the source code.

Next, we write down the following relations between wavenumbers

$$k_0 = \frac{c}{c_0} k, \; k_{0z} = \sqrt{\left(\frac{c}{c_0}\right)^2 k^2 - k_x^2 - k_y^2},$$

from which we conclude that $k_0 a \to \infty$ and $k_{0z} a \to \infty$ when $ka \to \infty$ for a fixed angle of incidence. Using these limits in (59), we conclude that $\langle B \rangle \to 0$ with one added assumption: the absolute value of the eigenvectors $|F_n|$ does not increase indefinitely for higher frequencies. This is reasonable because the norm of F_n is linked to the amplitude of the incident wave through the boundary condition (53), though we have not been able to demonstrate this formally.

In other words, the response from the particles averages to zero due to incoherence for high frequency, and the reflected wave sees only an empty halfspace with just the background matrix:

$$\langle R \rangle \to \zeta_R G.$$

It is possible to use this result to help calibrate an experimental measurement. As mentioned in the previous section, if we wish to use $\langle B \rangle$ to characterise the particles, we need to subtract $\zeta_R G$ from the average reflection coefficient $\langle R \rangle$. If the background matrix properties are not known, one could perform scattering experiments while increasing the frequency until the reflected wave response stops changing. At this point, the reflection coefficient would equal $\zeta_R G$.

8.3. Numerical results

In this section, we present some examples of numerical computations of the eigensystem (54) and the normalisation condition (57), using the Julia library [Gow24]. The main purpose of these numerical results is to show that the system is easily solvable for broad frequencies and volume fractions. We also demonstrate how sensitive reflection is to average particle size, which could be useful for designing characterisation experiments. All infinite summations over double indices defined in appendix A were truncated at $\ell = 2$ for numerical computations, and the absolute value of $\langle R \rangle$ is plotted in the figures in this section. This truncation provides a finite eigenvalue problem, which is solved numerically.

These calculations performed in Julia provide the effective wavenumber k_* and the eigenvectors F_n. We substitute the expressions for k_* and F_n into (56) to calculate the average backscattered amplitude $\langle B \rangle$, and then substitute $\langle B \rangle$ into (33)$_2$ to calculate the average reflection coefficient $\langle R \rangle$. To show how general the model is, and also provide some insight into the physics of the problem, we present three examples with very different material properties.

Case 1. We consider that the matrix is water, the exterior medium is a solid with acoustic properties $c = 3c_0$ and $\varrho = 3\varrho_0$, and particles some gas with $c_s = c_0/100$ and $\varrho_s = \varrho_0/100$. The reflection coefficients $\langle R \rangle$ are presented in figure 6 for the case of volume fraction $\phi = 10\%$.

In figure 6, the low frequency limit is computed with the formulas provided in [GK21], and the reflection coefficient of a homogeneous halfspace with no particles is given by $R = \zeta_R G$. The agreement between low
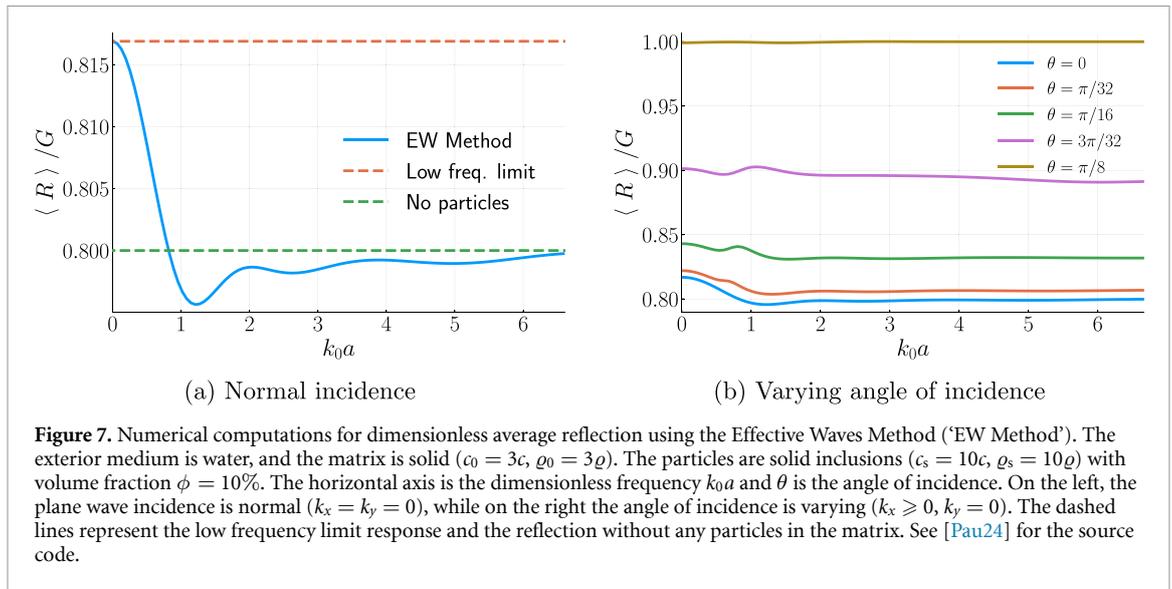
Figure 7. Numerical computations for dimensionless average reflection using the Effective Waves Method ('EW Method'). The exterior medium is water, and the matrix is solid ($c_0 = 3c$, $\varrho_0 = 3\varrho$). The particles are solid inclusions ($c_s = 10c$, $\varrho_s = 10\varrho$) with volume fraction $\phi = 10\%$. The horizontal axis is the dimensionless frequency $k_0 a$ and θ is the angle of incidence. On the left, the plane wave incidence is normal ($k_x = k_y = 0$), while on the right the angle of incidence is varying ($k_x \geqslant 0$, $k_y = 0$). The dashed lines represent the low frequency limit response and the reflection without any particles in the matrix. See [Pau24] for the source code.

frequency limit and the Effective Waves Method for $ka \ll 1$ is a good sanity check for the formulas for the normalisation condition (57).

Three main results can be obtained from figure 6: 1) The average reflection is sensitive to particle radius, with a drop of more than 50% in figure 6(a) if varying radius a for a fixed frequency ω; 2) we have numerical evidence that the high frequency limit matches the case with no particles; and 3) changing the angle of incidence in figure 6(b) only makes reflection less sensitive to particle radius. The last result suggests that normal incidence should be the optimal strategy to sense particle size if $\langle R \rangle$ can be measured with only one angle of incidence.

Case 2. We consider that the matrix is a solid medium ($c_0 = 3c$ and $\varrho_0 = 3\varrho$), and the exterior medium is water. In this case, we choose solid inclusions in the matrix such that $c_s = 10c$ and $\varrho_s = 10\varrho$. The results are presented in figure 7.

In this case 2, figure 7 shows the same qualitative behaviour as in figure 6. However, two observations must be made: 1) the average reflection is less sensitive to particle radius, with only a drop of about 3% in figure 7(a) when varying radius a for a fixed frequency ω; and 2) in figure 7(b), total reflection happens for angle of incidence θ bigger than the critical angle for the homogeneous matrix without particles, given by

$$\theta_c = \arcsin\left(\frac{c}{c_0}\right),$$

which for case 2 is equal to $\theta_c \approx 0.34 \text{rad} < \pi/8$.

Case 3. To study how reflection changes when varying the volume fraction of particles, defined in (58), we compute the average reflection coefficient for hard solid particles in water, $c_s = 100c$ and $\varrho_s = 100\varrho_0$. We take the exterior medium as a solid ($c = 3c_0$ and $\varrho = 3\varrho_0$). The results are presented in figure 8.

Figure 8 shows that the dependency of $\langle R \rangle$ with respect to volume fraction can be approximated by a simple linear relation. That suggests a first-order expansion in volume fraction would be accurate for reflection measurements for case 3 depicted in figure 8. We also notice that the slope of the curves in figure 8 is sensitive to radius a, which may be useful for sensing methods for the particle size distribution.

9. Conclusions

In this work, we solve an open challenge on how to calculate sound wave scattering from particles embedded in a matrix with different acoustic properties than the exterior medium. It seems we are the first to reach simple solvable equations, while retaining the same order of approximation as in the Quasi-Crystalline Approximation (QCA) [Lax52]. The QCA is one of the most successful approximations that captures multiple scattering between particles [MVV84, LM05, GPA19].

Figure 8. Numerical computations for dimensionless average reflection using the Effective Waves Method ('EW Method'). We have a hard powder in water ($c_s = 100c_0$, $\varrho_s = 100\varrho$) for some values of dimensionless frequent $k_0 a$. The horizontal axis is the volume fraction ϕ. The plane wave incidence is normal ($k_x = k_y = 0$) and the exterior medium is a solid ($c = 3c_0$, $\varrho = 3\varrho_0$). See [Pau24] for the source code.
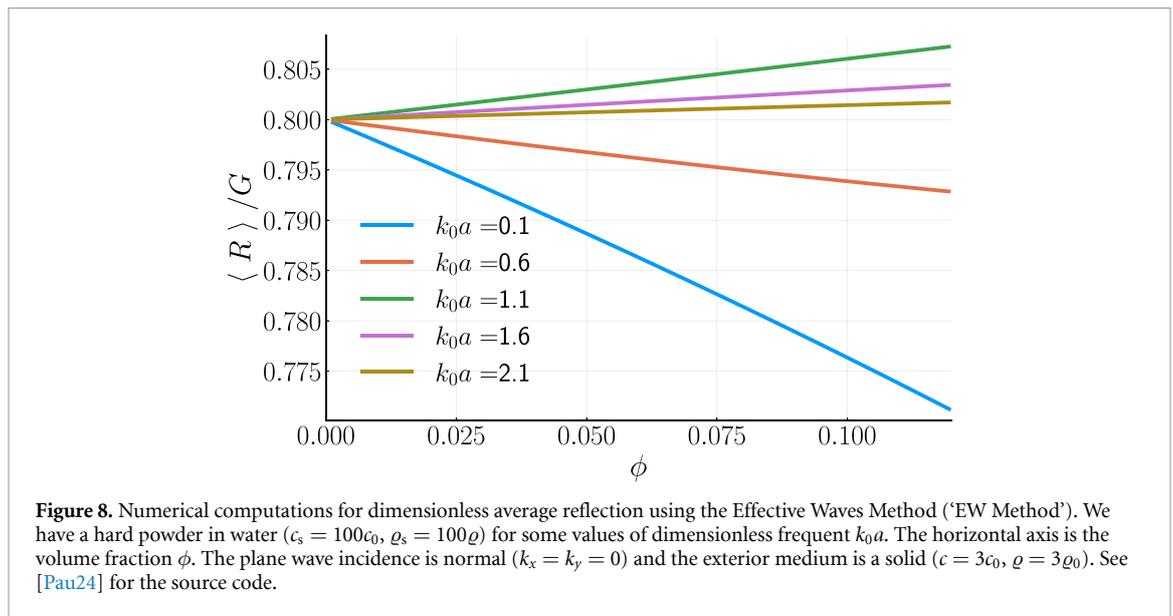
The method we develop can be applied to any material geometry, but for simplicity, we explore the simplest case in this paper: plane wave incidence on a halfspace.

Theoretical results. The key to solve for more than one background medium was to reformulate the QCA in terms of an approximation involving the field that excites each particle, as shown in (41). This reformulation shows that QCA is equivalent to averaging over self-interactions for all orders of multiple scattering. A similar interpretation has been noted before by [TPM11] by comparing QCA with a diagrammatic approximation given by Twersky [Twe64]. However, unlike the Twersky approximation, QCA does not discard any scattering contributions if defined as $(37)_{(1)}$ or (41). Instead, QCA averages over self-interactions. Our calculations confirm that, for a big class of ensembles presented in section 4, QCA is exact up to second-order scattering, as demonstrated in [MM08].

Our reformulation of QCA enabled us to reach simple solvable equations for the case of multiple background mediums, we call the extension of QCA to multiple mediums the eXtended Quasi-Crystalline Approximation (X-QCA). Using X-QCA leads to significant simplification in comparison to methods that use only QCA [KW20], and is applicable for a broad range of frequencies and particle properties.

Numerical results. To exemplify how the method works for a broad range of frequencies, volume fractions and material properties, we present explicit computations of the average reflection coefficient $\langle R \rangle$ in section 8.3. We show numerically that the average reflection coefficient can be sensitive to particle radius, depending on the material properties. This result can contribute to the development of sensing methods for particle size distribution of powders, emulsions, porous material or slurries.

We also give numerical evidence that, in the high frequency limit, there is no coherent reflection due to particles. This means the high frequency response can be used as calibration for equipment that uses the reflection coefficient to take measurements of particle scattering. If such measurements are not available, the simple measurement of reflected waves from the matrix with no particles can also be used as calibration, see discussion in section 6.1.

Possible generalisations. The model presented makes use of the Effective Waves Method [GK21], which allows any geometry or acoustic properties. The same procedure in this work can be used to compute the average wave scattering by a compact material filled with particles. On top of that, our method can be easily applied to any linear wave, including electromagnetic and elastic waves.

Future work. The method introduced here is not a mere theoretical curiosity. It is a necessary step before reaching quantifiable methods to measure particles in many areas of science and engineering. It is needed because, in almost any sensor setup, there will be different background mediums. To account for these mediums, and calculate the average reflection and transmission, one would need our results. A simple example is illustrated in figure 1 which involves a particulate flowing through a pipe past a sensor. In other words, a clear future avenue is to use the results here to develop sensors to predict the statistical properties of particulates from the measured reflection and transmission.

Other future avenues include validating our method (X-QCA) against high fidelity Monte Carlo simulations or experimental data. Another interesting step is to apply our results to design layered media containing particulates, as these can form functionally graded materials [Miy+99], which have applications in many areas like aerospace engineering, nuclear energy, optics, and others [LH18].

Data availability statement

The data that support the findings of this study are openly available at the following URL/DOI: https://doi.org/10.5281/zenodo.12797244.

Acknowledgment

Appendix A. Addition translation matrices

Here we provide the notation for addition translation matrices for spherical Bessel waves. For a translation $\boldsymbol{d}$ ($\boldsymbol{y} = \boldsymbol{x} + \boldsymbol{d}$), we have

$$
\begin{aligned}
\mathrm{v}_{\boldsymbol{n}}(\boldsymbol{y}) &= \sum_{\boldsymbol{n}'} \mathcal{V}_{\boldsymbol{n}\boldsymbol{n}'}(\boldsymbol{d}) \, \mathrm{v}_{\boldsymbol{n}'}(\boldsymbol{x}) \quad \forall\, \boldsymbol{x}, \boldsymbol{d} \in \mathbb{R}^3, \\
\mathrm{u}_{\boldsymbol{n}}(\boldsymbol{y}) &= \sum_{\boldsymbol{n}'} \mathcal{V}_{\boldsymbol{n}\boldsymbol{n}'}(\boldsymbol{d}) \, \mathrm{u}_{\boldsymbol{n}'}(\boldsymbol{x}) \quad \text{for } |\boldsymbol{x}| > |\boldsymbol{d}|, \\
\mathrm{u}_{\boldsymbol{n}}(\boldsymbol{y}) &= \sum_{\boldsymbol{n}'} \mathcal{U}_{\boldsymbol{n}\boldsymbol{n}'}(\boldsymbol{d}) \, \mathrm{v}_{\boldsymbol{n}'}(\boldsymbol{x}) \quad \text{for } |\boldsymbol{x}| < |\boldsymbol{d}|,
\end{aligned}
\tag{60}
$$

where the summations over double indices $\boldsymbol{n} = (\ell, m)$ represent double sums defined as

$$
\sum_{\boldsymbol{n}} := \sum_{\ell=0}^{\infty} \sum_{m=-\ell}^{\ell} .
$$

The addition translation matrices $\mathcal{V}_{\boldsymbol{n}\boldsymbol{n}'}(\boldsymbol{d})$ and $\mathcal{U}_{\boldsymbol{n}\boldsymbol{n}'}(\boldsymbol{d})$ are given by [GK21, equation (B.3)].

Appendix B. Regular spherical to plane waves

In this section, we determine the expression that connects the spherical Bessel waves representation of the regular field (21) with its planar wave representation (25). These expressions are only valid after the $L \to \infty$ limit in section 5.1. For that, we will use the following definition for the spherical harmonics

$$
Y_{(\ell,m)}(\hat{\boldsymbol{r}}) := (-1)^m \sqrt{\frac{2\ell+1}{4\pi} \frac{(\ell-m)!}{(\ell+m)!}} P_\ell^m(\cos\theta) \, \mathrm{e}^{im\phi},
$$

where P_ℓ^m are the usual associated Legendre polynomials.

We equate the averaged field expressed in both spherical Bessel (21) and planar representations (25), having in mind we chose k_{0z} such that $\langle A_- \rangle = 0$. This results in

$$
\langle A \rangle \mathrm{e}^{i\boldsymbol{k}_0 \cdot \boldsymbol{r}} = \sum_{\boldsymbol{n}} \langle g_{\boldsymbol{n}} \rangle \mathrm{v}_{\boldsymbol{n}}(k_0 \boldsymbol{r}) .
$$

Then, we substitute the planar wave expansion in terms of spherical Bessel waves, given by

$$
\mathrm{e}^{i\boldsymbol{k} \cdot \boldsymbol{r}} = 4\pi \sum_{\ell=0}^{\infty} \sum_{m=-\ell}^{\ell} i^\ell \overline{Y_{(\ell,m)}}(\hat{\boldsymbol{k}}) \, \mathrm{v}_{(\ell,m)}(k\boldsymbol{r}) ,
\tag{61}
$$

where the overline denotes complex conjugation. The final step is to use the orthogonality relations of the spherical harmonics, which leads to

$$
\langle g_{\boldsymbol{n}} \rangle = C_{\boldsymbol{n}} \langle A \rangle ,
\tag{62}
$$

where we have defined

$$C_{(\ell,m)} := 4\pi \, i^{\ell} \, \overline{Y_{(\ell,m)}} \left(\hat{\boldsymbol{k}}_0 \right).$$

(63)

Appendix C. Translation symmetry

In the limit of an infinite number of particles (see section 5.1), the average regular field can be represented by a plane wave, given by (25). Then, its dependency on x and y is given only by a known complex phase. For a general translation in the $z = 0$ plane of $\boldsymbol{b} = x_0 \hat{\boldsymbol{x}} + y_0 \hat{\boldsymbol{y}}$, we have

$$\langle u_{\text{reg}}(\boldsymbol{r}+\boldsymbol{b}) \rangle = \langle u_{\text{reg}}(\boldsymbol{r}) \rangle e^{i\boldsymbol{k}_0 \cdot \boldsymbol{b}} = \sum_{\boldsymbol{n}'} \langle g_{\boldsymbol{n}'} \rangle \text{v}_{\boldsymbol{n}'}(k_0 \boldsymbol{r}) e^{i\boldsymbol{k}_0 \cdot \boldsymbol{b}},$$

$$\langle u_{\text{reg}}(\boldsymbol{r}+\boldsymbol{b}) \rangle = \sum_{\boldsymbol{n}} \langle g_{\boldsymbol{n}} \rangle \text{v}_{\boldsymbol{n}}(k_0 \boldsymbol{r} + k_0 \boldsymbol{b}) = \sum_{\boldsymbol{n}\boldsymbol{n}'} \langle g_{\boldsymbol{n}} \rangle \mathcal{V}_{\boldsymbol{n}\boldsymbol{n}'}(k_0 \boldsymbol{b}) \, \text{v}_{\boldsymbol{n}'}(k_0 \boldsymbol{r}),$$

where we have used (21) in both equations above, and translation matrices in appendix A in the second line. Equating both lines above, and using the orthogonality relations of spherical harmonics, we conclude that

$$\langle g_{\boldsymbol{n}} \rangle e^{i\boldsymbol{k}_0 \cdot \boldsymbol{b}} = \sum_{\boldsymbol{n}'} \langle g_{\boldsymbol{n}'} \rangle \mathcal{V}_{\boldsymbol{n}'\boldsymbol{n}}(k_0 \boldsymbol{b}),$$

(64)

Then, we perform the same translation of $\boldsymbol{b}$ in (38) to get

$$\langle f_{\boldsymbol{n}} \rangle (\boldsymbol{r}_1 + \boldsymbol{b}) = T_{\boldsymbol{n}} \sum_{\boldsymbol{n}'} \langle g_{\boldsymbol{n}'} \rangle \mathcal{V}_{\boldsymbol{n}'\boldsymbol{n}}(k_0 \boldsymbol{r}_1 + \boldsymbol{b})$$

$$+ \mathfrak{n} \, T_{\boldsymbol{n}} \sum_{\boldsymbol{n}'} \int_{\mathcal{R}_a \backslash \mathcal{B}(\boldsymbol{r}_1 + \boldsymbol{b}, 2a)} \mathcal{U}_{\boldsymbol{n}'\boldsymbol{n}}(k_0 \boldsymbol{r}_1 - k_0 \boldsymbol{r}_2 + k_0 \boldsymbol{b}) \langle f_{\boldsymbol{n}'} \rangle (\boldsymbol{r}_2) \, \mathrm{d}\boldsymbol{r}_2.$$

We decompose the regular translation matrix into two factors (see [GK21, eq. (B.3)]) and perform the change of variables $\boldsymbol{r}_2 \to \boldsymbol{r}'_2 = \boldsymbol{r}_2 - \boldsymbol{b}$ into the above to reach

$$\langle f_{\boldsymbol{n}} \rangle (\boldsymbol{r}_1 + \boldsymbol{b}) = T_{\boldsymbol{n}} \sum_{\boldsymbol{n}'\boldsymbol{n}''} \langle g_{\boldsymbol{n}'} \rangle \mathcal{V}_{\boldsymbol{n}'\boldsymbol{n}''}(k_0 \boldsymbol{b}) \, \mathcal{V}_{\boldsymbol{n}''\boldsymbol{n}}(k_0 \boldsymbol{r}_1)$$

$$+ \mathfrak{n} \, T_{\boldsymbol{n}} \sum_{\boldsymbol{n}'} \int_{\mathcal{R}_a \backslash \mathcal{B}(\boldsymbol{r}_1, 2a)} \mathcal{U}_{\boldsymbol{n}'\boldsymbol{n}}(k_0 \boldsymbol{r}_1 - k_0 \boldsymbol{r}'_2) \langle f_{\boldsymbol{n}'} \rangle (\boldsymbol{r}'_2 + \boldsymbol{b}) \, \mathrm{d}\boldsymbol{r}'_2.$$

Finally, we substitute (64) in the above, leading to

$$\langle f_{\boldsymbol{n}} \rangle (\boldsymbol{r}_1 + \boldsymbol{b}, \lambda) = T_{\boldsymbol{n}} \sum_{\boldsymbol{n}''} \langle g_{\boldsymbol{n}''} \rangle \mathcal{V}_{\boldsymbol{n}''\boldsymbol{n}}(k_0 \boldsymbol{r}_1) \, e^{i\boldsymbol{k}_0 \cdot \boldsymbol{b}}$$

$$+ \mathfrak{n} \, T_{\boldsymbol{n}} \sum_{\boldsymbol{n}'} \int_{\mathcal{R}_a \backslash \mathcal{B}(\boldsymbol{r}_1, 2a)} \mathcal{U}_{\boldsymbol{n}'\boldsymbol{n}}(k_0 \boldsymbol{r}_1 - k_0 \boldsymbol{r}'_2) \langle f_{\boldsymbol{n}'} \rangle (\boldsymbol{r}'_2 + \boldsymbol{b}) \, \mathrm{d}\boldsymbol{r}'_2,$$

which is the same equation as (38), but written in terms of $\langle f_{\boldsymbol{n}} \rangle (\boldsymbol{r}_1 + \boldsymbol{b}) = \langle f_{\boldsymbol{n}} \rangle (\boldsymbol{r}_1) e^{i\boldsymbol{k}_0 \cdot \boldsymbol{b}}$ instead of $\langle f_{\boldsymbol{n}} \rangle (\boldsymbol{r}_1)$. Assuming the uniqueness of the solution for (38), one can deduce that

$$\langle f_{\boldsymbol{n}} \rangle (\boldsymbol{r}_1) = \langle f_{\boldsymbol{n}} \rangle (0, 0, z_1) \, e^{i\left(k_x x_1 + k_y y_1\right)},$$

(65)

and we have reduced the dimensions of our integral equation from three to one, due to symmetry.

Appendix D. Outgoing spherical to plane waves

To simplify (26), we use (65) from appendix C, which leads to

$$\lim_{\substack{J \to \infty \\ L \to \infty}} \sum_{i} \langle u_{\text{sc}}^i(\boldsymbol{r}) \rangle = \mathfrak{n} \sum_{\boldsymbol{n}} \int_{a+\delta}^{\infty} \langle f_{\boldsymbol{n}} \rangle (0, 0, z_1) \, I_{\boldsymbol{n}}(\boldsymbol{r}, z_1) \, \mathrm{d}z_1,$$

(66)

where we have defined the following quantity that can be determined analytically:

$$I_{\boldsymbol{n}}(\boldsymbol{r}, z_1) := \int_{\mathbb{R}^2} \text{u}_{\boldsymbol{n}}(k_0 \boldsymbol{r} - k_0 \boldsymbol{r}_1) \, e^{i\left(k_x x_1 + k_y y_1\right)} \mathrm{d}x_1 \mathrm{d}y_1, \quad z \neq z_1,$$

(67)

and results in a plane wave in the z_1 direction. To simplify (67), we use the following transformation formula [DM65, BKS91, Kri16, Kri79, GK21]

$$\mathrm{u}_{\boldsymbol{n}}\left(k_0\boldsymbol{r}\right) = \mathrm{u}_{(\ell,m)}\left(k_0\boldsymbol{r}\right) = \frac{1}{2\pi\,\mathrm{i}^\ell}\int_{\mathbb{R}^2}\frac{\mathrm{Y}_{\boldsymbol{n}}\left(\hat{\boldsymbol{q}}\right)}{k_0 q_z}\mathrm{e}^{\mathrm{i}\boldsymbol{q}\cdot\boldsymbol{r}}\mathrm{d}q_x\mathrm{d}q_y,\quad z>0,$$

where $\boldsymbol{q} = (q_x, q_y, q_z)$ with $q_x^2 + q_y^2 + q_z^2 = k_0^2$. We substitute the above into (67) and perform the following calculations for $z > z_1$ as follows:

$$
\begin{aligned}
I_{\boldsymbol{n}}\left(\boldsymbol{r},z_1\right) &= \frac{1}{2\pi\,\mathrm{i}^\ell}\int_{\mathbb{R}^2}\left[\int_{\mathbb{R}^2}\frac{\mathrm{Y}_{\boldsymbol{n}}\left(\hat{\boldsymbol{q}}\right)}{k_0 q_z}\mathrm{e}^{\mathrm{i}\boldsymbol{q}\cdot(\boldsymbol{r}-\boldsymbol{r}_1)+\mathrm{i}\left(k_x x_1 + k_y y_1\right)}\mathrm{d}q_x\mathrm{d}q_y\right]\mathrm{d}x_1\mathrm{d}y_1 \\
&= \frac{1}{2\pi\,\mathrm{i}^\ell}\int_{\mathbb{R}^2}\frac{\mathrm{Y}_{\boldsymbol{n}}\left(\hat{\boldsymbol{q}}\right)}{k_0 q_z}\mathrm{e}^{\mathrm{i}\boldsymbol{q}\cdot\boldsymbol{r}-\mathrm{i}q_z z_1}\left[\int_{-\infty}^{\infty}\mathrm{e}^{\mathrm{i}(k_x-q_x)x_1}\mathrm{d}x_1\int_{-\infty}^{\infty}\mathrm{e}^{\mathrm{i}(k_y-q_y)y_1}\mathrm{d}y_1\right]\mathrm{d}q_x\mathrm{d}q_y \\
&= \frac{2\pi}{\mathrm{i}^\ell k_0}\int_{\mathbb{R}^2}\frac{\mathrm{Y}_{\boldsymbol{n}}\left(\hat{\boldsymbol{q}}\right)}{q_z}\mathrm{e}^{\mathrm{i}(\boldsymbol{q}\cdot\boldsymbol{r}-q_z z_1)}\delta\left(q_x-k_x\right)\delta\left(q_y-k_y\right)\mathrm{d}q_x\mathrm{d}q_y \\
&= \frac{2\pi\,\mathrm{i}^{-\ell}}{k_0 k_{0z}}\mathrm{Y}_{\boldsymbol{n}}\left(\hat{\boldsymbol{k}}\right)\mathrm{e}^{\mathrm{i}\left(k_x x + k_y y\right)+\mathrm{i}k_{0z}(z-z_1)},
\end{aligned}
\tag{68}
$$

where we have changed the order of integration, and used the Fourier expansion of the Dirac delta distribution:

$$\delta\left(q\right) = \frac{1}{2\pi}\int_{-\infty}^{\infty}\mathrm{e}^{-\mathrm{i}qx}\mathrm{d}x.$$

For the case $z < z_1$, we use the fact that

$$I_{\boldsymbol{n}}\left(\boldsymbol{r},z_1\right) = (-1)^\ell\int_{\mathbb{R}^2}\mathrm{u}_{\boldsymbol{n}}\left(k_0\boldsymbol{r}_1 - k_0\boldsymbol{r}\right)\mathrm{e}^{\mathrm{i}\left(k_x x_1 + k_y y_1\right)}\mathrm{d}x_1\mathrm{d}y_1,\quad z\neq z_1,$$

and we repeat the same computations in (68) to reach

$$I_{\boldsymbol{n}}\left(\boldsymbol{r},z_1\right) = \frac{2\pi\,\mathrm{i}^\ell}{k_0 k_{0z}}\mathrm{Y}_{\boldsymbol{n}}\left(\hat{\boldsymbol{k}}_0\right)\mathrm{e}^{\mathrm{i}\left(k_x x + k_y y\right)+\mathrm{i}k_{0z}(z_1-z)}.\tag{69}$$

Substituting (69) into (66), we conclude that the sum of the average scattered waves by particles (24) can also be represented as a plane wave in the region $0 < z < \delta$. The results of this appendix motivate the definition of the average backscattered amplitude $\langle B\rangle$ in (28).

ORCID iDs

Paulo S Piva ● https://orcid.org/0000-0002-8239-970X
Art L Gower ● https://orcid.org/0000-0002-3229-5451

References

[Fol45] Foldy L L 1945 The multiple scattering of waves. I. General theory of isotropic scattering by randomly distributed scatterers *Phys. Rev.* **67** 107–19

[Lax52] Lax M 1952 Multiple scattering of waves. II. The effective field in dense systems *Phys. Rev.* **85** 621–9

[WT61] Waterman P C and Truell R 1961 Multiple scattering of waves *J. Math. Phys.* **2** 512–37

[Hua63] Huang K 1963 *Statistical Mechanics* (Wiley)

[FW64] Fikioris J G and Waterman P C 1964 Multiple scattering of waves. II. "Hole corrections" in the scalar case *J. Math. Phys.* **5** 1413–20

[Twe64] Twersky V 1964 On propagation in random media of discrete scatterers *Proc. Symp. Appl. Math* vol 16 pp 84–116

[DM65] Danos M and Maximon L C 1965 Multipole matrix elements of the translation operator *J. Math. Phys.* **6** 766–78

[Ado71] Adomian G 1971 The closure approximation in the hierarchy equations *J. Stat. Phys.* **3** 127–33

[Wat71] Waterman P C 1971 Symmetry, unitarity and geometry in electromagnetic scattering *Phys. Rev.* D **3** 825–39

[VVP78] Varadan V K, Varadan V V and Pao Y H 1978 Multiple scattering of elastic waves by cylinders of arbitrary cross section. I. SH waves *J. Acoust. Soc. Am.* **63** 1310–9

[Kri79] Kristensson G 1979 Electromagnetic scattering from a buried three-dimensional inhomogeneity in a lossy ground *Technical Report* Institute of Theoretical Physics, Chalmers University of Technology 79-29

[Wil81] Willis J R 1981 Variational principles for dynamic problems for inhomogeneous elastic media *Wave Motion* **3** 1–11

[MVV84] Ma Y, Varadan V V and Varadan V K 1984 Multiple scattering theory for wave propagation in discrete random media *Int. J. Eng. Sci.* **22** 1139–48

[HBE87] Hynne F, Bullough R K and Edwards S F 1987 The scattering of light. II. The complex refractive index of a molecular fluid *Phil. Trans. R. Soc.* A **321** 305–60

[BKS91] Bostrom A, Kristensson G and Strom S 1991 Transformation properties of plane, spherical and cylindrical scalar and vector wave functions *Field Representations and Introduction to Scattering Acoustic, Electromagnetic and Elastic Wave Scattering V V* Varadan A Lakhtakia V K Varadan pp 165–210

[MTM96] Mishchenko M I, Travis L D and Mackowski D W 1996 T-matrix computations of light scattering by nonspherical particles: a review *J. Quant. Spectrosc. Radiat. Transfer* **55** 535–75

[Miy+99] Miyamoto Y, Kaysser W A, Rabin B H, Kawasaki A and Ford R G 1999 'Functionally graded materials: design, processing and applications

[Kon+04] Kong J A, Tsang L, Ding K-H and Ao C O 2004 *Scattering of Electromagnetic Waves: Numerical Simulations* (Wiley)

[Cha+05] Challis R E, Povey M J W, Mather M L and Holmes A K 2005 Ultrasound techniques for characterizing colloidal dispersions *Rep. Prog. Phys.* **68** 1541

[Gar+05] Garcia-Valenzuela A, Barrera R G, Sanchez-Perez C, Reyes-Coronado A and Mendez E R 2005 Coherent reflection of light from a turbid suspension of particles in an internal-reflection configuration: Theory versus experiment *Opt. Express* **13** 6723–37

[LM05] Linton C M and Martin P A 2005 Multiple scattering by random configurations of circular cylinders: Second-order corrections for the effective wavenumber *J. Acoust. Soc. Am.* **117** 3413–23

[LM06] Linton C and Martin P 2006 Multiple scattering by multiple spheres: a new proof of the Lloyd–Berry formula for the effective wavenumber *SIAM J. Appl. Math.* **66** 1649–68

[MM08] Martin P and Maurel A 2008 Multiple scattering by random configurations of circular cylinders: weak scattering without closure assumptions *Wave Motion* **45** 865–80

[PA10] Parnell W and Abrahams I 2010 Multiple point scattering to determine the effective wavenumber and effective material properties of an inhomogeneous slab *Waves Random Complex Media* **20** 678–701

[CPS11] Chung C -W, Popovics J S and Struble L J 2011 Flocculation and sedimentation in suspensions using ultrasonic wave reflection *J. Acoust. Soc. Am.* **129** 2944–51

[TPM11] Tishkovets V P, Petrova E V and Mishchenko M I 2011 Scattering of electromagnetic waves by ensembles of particles and discrete random media *J. Quant. Spectrosc. Radiat. Transfer* **112** 2095–127

[CDW12] Caleap M, Drinkwater B W and Wilcox P D 2012 Effective dynamic constitutive parameters of acoustic metamaterials with random microstructure *New J. Phys.* **14** 033014

[CD15] Caleap M and Drinkwater B W 2015 Metamaterials: supra-classical dynamic homogenization* *New J. Phys.* **17** 123022

[AC15] Al-Lashi R S and Challis R E 2015 Ultrasonic particle sizing in aqueous suspensions of solid particles of unknown density *J. Acoust. Soc. Am.* **138** 1023–9

[FHP16] Forrester D M, Huang J and Pinfield V J 2016 Characterisation of colloidal dispersions using ultrasound spectroscopy and multiple-scattering theory inclusive of shear-wave effects *Chem. Eng. Res. Design* **114** 69–78

[Kri16] Kristensson G 2016 *Scattering of Electromagnetic Waves by Obstacles* (*Mario Boella Series on Electromagnetism in Information and Communication*) (SciTech Publishing)

[Kue16] Kuehn C 2016 Moment closure-a brief review *Control of Self-Organizing Nonlinear Systems* (Springer International Publishing) pp 253–71

[Mis+16] Mishchenko M I, Dlugach J M, Yurkin M A, Bi L, Cairns B, Liu L, Panetta R L, Travis L D, Yang P and Zakharova N T 2016 First-principles modeling of electromagnetic scattering by discrete and discretely heterogeneous random media *Phys. Rep.* **632** 1–75

[20917] ISO 36BI 20998-3:2017 2017 Measurement and characterization of particles by acoustic methods London: British Standards Institution

[DM18] Doicu A and Mishchenko M I 2018 Overview of methods for deriving the radiative transfer theory from the Maxwell equations. I: approach based on the far-field Foldy equations *J. Quant. Spectrosc. Radiat. Transfer* **220** 123–39

[Gow+18] Gower A L, Smith M J A, Parnell W J and Abrahams I D 2018 Reflection from a multi-species material and its transmitted effective wavenumber *Proc. R. Soc.* A **474** 20170864

[LH18] Li W and Han B 2018 Research and application of functionally gradient materials *IOP Conf. Ser.: Mater. Sci. Eng.* **394** 022065

[GPA19] Gower A L, Parnell W J and Abrahams I D 2019 Multiple waves propagate in random particulate materials *SIAM J. Appl. Math.* **79** 2569–92

[Wil19] Willis J R 2019 Transmission and reflection of waves at an interface between ordinary material and metamaterial *J. Mech. Phys. Solids* **136** 103678

[KS20] Kolomietz V M and Shlomo S 2020 *Mean Field Theory* (World Scientific Publishing Company)

[KW20] Kristensson G and Wellander N 2020 Multiple scattering by a collection of randomly located obstacles distributed in a dielectric slab *Advances in Mathematical Methods for Electromagnetics*

[MS20] Martin P A and Skvortsov A T 2020 Scattering by a sphere in a tube and related problems *J. Acoust. Soc. Am.* **148** 191–200

[Wil20] Willis J R 2020 Transmission and reflection at the boundary of a random two-component composite *Proc. R. Soc.* A **476** 20190811

[Faw21] Fawcett J A 2021 The effective medium for a cylinder with cylindrical inclusions *J. Acoust. Soc. Am.* **150** 2600–12

[GK21] Gower A L and Kristensson G 2021 Effective waves for random three-dimensional particulate materials *New J. Phys.* **23** 063083

[GHK23] Gower A L, Hawkins S C and Kristensson G 2023 A model to validate effective waves in random particulate media: spherical symmetry *Proc. R. Soc.* A **479** 44

[Wil23] Willis J R 2023 Transmission and reflection of energy at the boundary of a random two-component composite *Proc. R. Soc.* A **479** 20220730

[GD24] Gower A L and Deakin J 2024 MultipleScatering.jl: a Julia library for simulating, processing, and plotting multiple scattering of waves. Version 0.1.21 (available at: https://github.com/JuliaWaveScattering/MultipleScattering.jl)

[Gow24] Gower A L 2024 Effectivewaves.jl: a julia package to calculate ensemble averaged waves in heterogeneous materials. Version 0.3.6 (available at: https://github.com/JuliaWaveScattering/EffectiveWaves.jl)

[KPG24] Karnezis A, Piva P S and Gower A L 2024 The average transmitted wave in random particulate materials *New J. Phys.* **26** 063002

[NPG24] Napal K K, Piva P S and Gower A L 2024 Effective T-matrix of a cylinder filled with a random two-dimensional particulate *Proc. R. Soc.* A **480** 20230660

[Sim+24] Simon A, Baudis Q, Wunenburger R and Valier-Brasier T 2024 Propagation of elastic waves in correlated dispersions of resonant scatterers *J. Acoust. Soc. Am.* **155** 3627–38

[Piv24] Piva P S 2024 Acoustic waves in a halfspace material filled with random particulate: scripts for numerical results and figures, repository name *Zenodo* https://doi.org/10.5281/zenodo.12797244